AD-A122 388 SPECTRAL MEASUREMENTS OF REFLECTANCE RADIANCE AND EMISSIVITY(U) ARMY ENGINEER WATERWAYS EXPERIMENT STATION VICKSBURG MS ENVIRONMENTAL LAB G HUEBNER 1/1

UNCLASSIFIED OCT 82 WES/TR/EL-82-8 F/G 17/4 NL

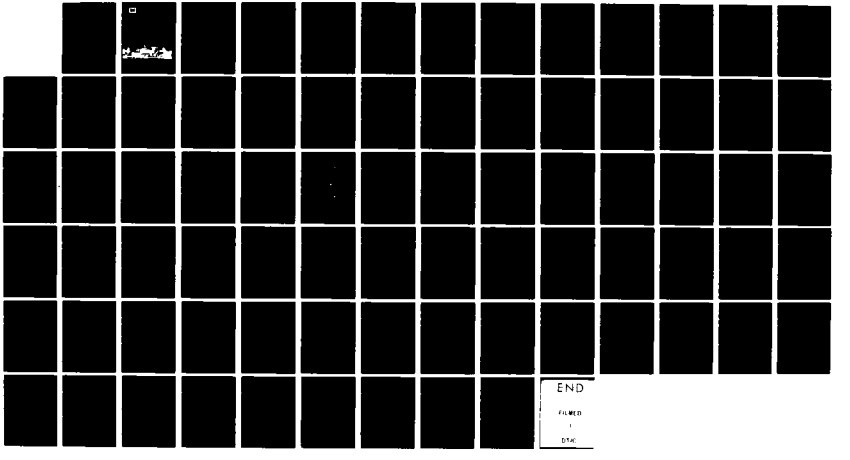

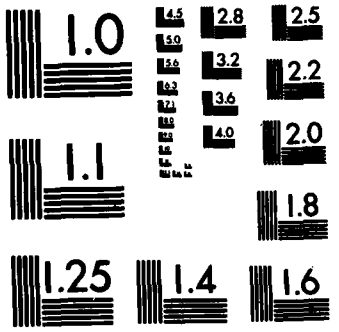

MICROCOPY RESOLUTION TEST CHART
NATIONAL BUREAU OF STANDARDS-1963-A

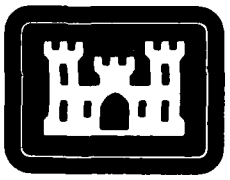

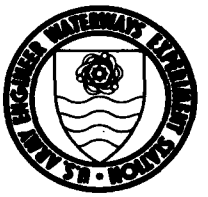

TECHNICAL REPORT EL-82-8

SPECTRAL MEASUREMENTS OF REFLECTANCE, RADIANCE, AND EMISSIVITY

by

Gunter Hübner

Environmental Laboratory
U. S. Army Engineer Waterways Experiment Station
P. O. Box 631, Vicksburg, Miss. 39180

October 1982

Final Report

Prepared for Office, Chief of Engineers, U. S. Army
Washington, D. C. 20314

Under Project No. 4A762730AT42, Task E3,
Work Unit 002

Destroy this report when no longer needed. Do not return it to the originator.

The findings in this report are not to be construed as an official Department of the Army position unless so designated by other authorized documents.

The contents of this report are not to be used for advertising, publication, or promotional purposes. Citation of trade names does not constitute an official endorsement or approval of the use of such commercial products.

Unclassified

SECURITY CLASSIFICATION OF THIS PAGE (When Data Entered)

REPORT DOCUMENTATION PAGE	READ INSTRUCTIONS BEFORE COMPLETING FORM
1. REPORT NUMBER Technical Report EL-82-8	2. GOVT ACCESSION NO. A122388 3. RECIPIENT'S CATALOG NUMBER
4. TITLE (and Subtitle) SPECTRAL MEASUREMENTS OF REFLECTANCE, RADIANCE, AND EMISSIVITY	5. TYPE OF REPORT & PERIOD COVERED Final report 6. PERFORMING ORG. REPORT NUMBER
7. AUTHOR(s) Gunter Hübner	8. CONTRACT OR GRANT NUMBER(s)
9. PERFORMING ORGANIZATION NAME AND ADDRESS U. S. Army Engineer Waterways Experiment Station Environmental Laboratory P. O. Box 631, Vicksburg, Miss. 39180	10. PROGRAM ELEMENT, PROJECT, TASK AREA & WORK UNIT NUMBERS Project No. 4A762730AT42, Task E3, Work Unit 002
11. CONTROLLING OFFICE NAME AND ADDRESS Office, Chief of Engineers, U. S. Army Washington, D. C. 20314	12. REPORT DATE October 1982 13. NUMBER OF PAGES 72
14. MONITORING AGENCY NAME & ADDRESS(if different from Controlling Office)	15. SECURITY CLASS. (of this report) Unclassified 15a. DECLASSIFICATION/DOWNGRADING SCHEDULE

16. DISTRIBUTION STATEMENT (of this Report)

Approved for public release; distribution unlimited.

17. DISTRIBUTION STATEMENT (of the abstract entered in Block 20, if different from Report)

18. SUPPLEMENTARY NOTES

Available from National Technical Information Service, 5285 Port Royal Road, Springfield, Va. 22151

19. KEY WORDS (Continue on reverse side if necessary and identify by block number)

Camouflage
Military geographic intelligence
Military operations
Spectrum analysis

20. ABSTRACT (Continue on reverse side if necessary and identify by block number)

An important concept in military camouflage is to match the radiative surface properties of targets with those of the background. This match has to be accomplished over a wide range of the electromagnetic spectrum as well as for a range of weather conditions. The first step in the matching procedure is to measure the surface properties of targets and backgrounds. This report documents research for developing a capability to measure radiative surface

(Continued)

DD FORM 1 JAN 73 1473 EDITION OF 1 NOV 65 IS OBSOLETE

Unclassified

SECURITY CLASSIFICATION OF THIS PAGE (When Data Entered)

20. ABSTRACT (Continued)

properties in the visual, near infrared, and thermal infrared portions of the electromagnetic spectrum.

The measurements were done with a Barnes SpectralMaster Infrared Research Radiometer, Model 12-550. This report explains the procedure developed in-house for calibrating the instrument and suggests procedures for measuring reflectance, radiance, and emissivity. To illustrate the procedures, measurements of sand and rock samples from Moab, Utah, are included.

PREFACE

The study reported herein was conducted at the U. S. Army Engineer Waterways Experiment Station (WES) from February to December 1981 under Department of the Army Project No. 4A762730AT42, Task E3, Work Unit 002, Electromagnetic Target Surround Characteristics in Natural Terrains.

The study was conducted under the general supervision of Dr. John Harrison, Chief of the Environmental Laboratory (EL), and Mr. Bob Benn, Chief of the Environmental Systems Division, EL, and under the direct supervision of Dr. Lewis E. Link, Jr., Chief of the Environmental Constraints Group, EL. The work reported here was accomplished and this report prepared by Dr. Gunter Hübner, Industrieanlagen--Betriebsgesellschaft, Ottobrunn, Federal Republic of Germany, during his assignment to WES under a Government-sponsored scientific exchange program.

Commanders and Directors of WES during the study and the preparation of this report were COL Nelson P. Conover, CE, and COL Tilford C. Creel, CE. Technical Director was Mr. F. R. Brown.

This report should be cited as follows:

> Hübner, Gunter. 1982. "Spectral Measurements of Reflectance, Radiance, and Emissivity," Technical Report EL-82-8, U. S. Army Engineer Waterways Experiment Station, CE, Vicksburg, Miss.

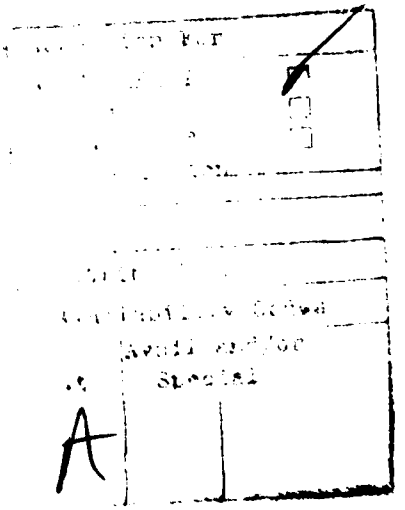

CONTENTS

CONVERSION FACTORS, INCH-POUND TO METRIC (SI) UNITS OF MEASUREMENT

Inch-pound units of measurement used in this report can be converted to metric (SI) units as follows:

Multiply	By	To Obtain
degrees (angle)	0.01745	radians
inches	25.4	millimetres
pounds (force)	4.448	newtons
pounds (force) per square inch (psi)	6895	pascals

SPECTRAL MEASUREMENTS OF REFLECTANCE, RADIANCE, AND EMISSIVITY

PART I: INTRODUCTION

Background

1. The Environmental Systems Division of the Environmental Laboratory at the U. S. Army Engineer Waterways Experiment Station (WES) is interested in determining the effects of the environment on military activities, a specific aspect of which is the development of camouflage of fixed installations.

2. The usual aim of camouflage is not to make an object invisible, but to match the radiations of target and background. If a good match is achieved, it will be difficult to locate and acquire the target.

3. Historically, the only radiation relevant for camouflage was visible light, with the human eye being the sensor to defeat. However, man-made sensors have become available which extend the threat to other parts of the electromagnetic spectrum. These include the near infrared, with wavelengths 0.7 to 1.2 μm, and the thermal infrared, with wavelengths 2 to 20 μm.

4. Radiation received by a sensor from target and background is emitted and/or reflected radiation. If a scene is illuminated by a light source, e.g. the sun, radiation incident on the scene is reflected and can be detected by a sensor. Target and background can be discriminated by differences in reflectance. In the thermal infrared, scene components emit radiation, too. Emitted intensity depends on the temperature and the emissivity of the surface. Hence, reflectance and emissivity are characteristic surface properties describing the radiation exchange of the surface.

5. To address the problems of fixed installation camouflage, WES conducts an active program to collect signatures of targets and backgrounds. Models have been developed to predict the signatures for times and situations where data collection is not possible. The models require

surface characteristics such as reflectance and emissivity as input parameters.

Objective and Scope

6. The objective of the work reported here was to develop a capability to measure quantitatively radiation intensities in the visible and infrared parts of the spectrum in order to determine radiative surface properties.

7. Suitable instrumentation, a Barnes SpectralMaster Infrared Research Radiometer Model 12-550, was purchased in 1976. However, a concerted effort to extract useful data from the instrument had not been made. Calibration of the instrument was considerably more complicated than what had been expected by previous operators. In 1981, the author made a determined effort to bring the instrument up to its capabilities and succeeded.

8. The primary contribution of this report is the detailed description given in Part II of the methods used to calibrate the instrument. Results of sample measurements are included in Part IV.

9. Readers of this report who are interested only in using the instrument will profit most from Part III, which describes the procedure for measuring specific properties, and Appendix A, which lists an operating sequence for the instrument.

PART II: INSTRUMENT CALIBRATION

Description of Instrument

10. The instrument used and described here is a Barnes Spectral-Master Infrared Research Radiometer Model 12-550. It is designed to perform advanced radiometric research in industrial, scientific, and defense applications. It consists of a sensing head and an electronic control unit. A more detailed description than what follows is found in the instruction manual of the instrument (Barnes 1977).

11. In the sensing head, radiation from the selected target is collected by a Cassegrain-type optical system and focused on a plane that includes a field-limiting aperture and a radiation chopper. Transfer mirrors refocus the expanding radiation beam on the plane of a spectral filter assembly, and a relay lens refocuses the energy upon the detector. Here, the radiation signal is transformed into an electrical signal that bears information concerning the magnitude of the radiation signal and its variations. A preamplifier amplifies this signal to a level and impedance suitable for transmission through a cable to the remote electronics unit.

12. In the electronic control unit, solid-state electronics amplify, demodulate, and filter the detector signal. The result is an output voltage having an amplitude that can be directly related to the absolute radiation from the target. Moreover, variations in this electrical signal reproduce the variations in the target of interest. The electrical output signal is displayed on the front panel meter. When the SpectralMaster is equipped with a motor-driven circular variable filter, the instrument supplies high-speed, continuous spectral measurements over a selected wavelength range. If the signals are fed into an X-Y plotter, spectral characteristics curves are plotted as a function of wavelength.

13. The instrument can be fitted with several interchangeable modules designed to cover different parts of the electromagnetic spectrum. The following detectors and filter wheels were available for this work:

Detector	Detector Temperature	Wheel	Spectral Range
Si	Ambient	Visual and near infrared	0.4-1.1 μm
InSb	77° K	Infrared	2.5-5.5 μm
HgCdTe	77° K	Infrared	3.0-14.0 μm

14. The X-Y plotter receives two signals from the SpectralMaster, one for the X-axis and one for the Y-axis. The signal for the X-axis is a voltage which depends on the position of the filter wheel. This voltage has to be related to the wavelength of the filter by a procedure which is described under the next center heading. The signal for the Y-axis of the plotter is the amplified detector signal. To relate this signal quantitatively to the radiation intensity seen by the detector, the relative response of the detector and its transfer function have to be determined. This will be described in paragraphs 40 through 58.

Calibration of the Wavelength Scale

15. The filter housing protrudes from the optical head and has a viewing window which shows a scale marked in terms of angular rotation: d = 0...360°.* The instrument includes provisions for remote indication of filter position by means of an electrical output signal. The filter wheel is connected to a potentiometer that produces an output voltage of 0 volts DC for 0° effective rotation and 26 volts DC for 360° effective rotation. The difference in voltage between these (slightly separated) points is a fairly linear function of angular rotation. Thus a remote voltmeter, recorder, or other device can be used to provide an indication of wheel position in terms of angular rotation.

Infrared filter

16. The measured relationship between the dial reading d of the infrared filter and the output voltage V_x is shown in Figure 1. A regression line through 12 measured points gives a linear correlation coefficient of $\rho = 0.999998$ and a regression line

* A table of factors for converting inch-pound to metric (SI) units is presented on page 3.

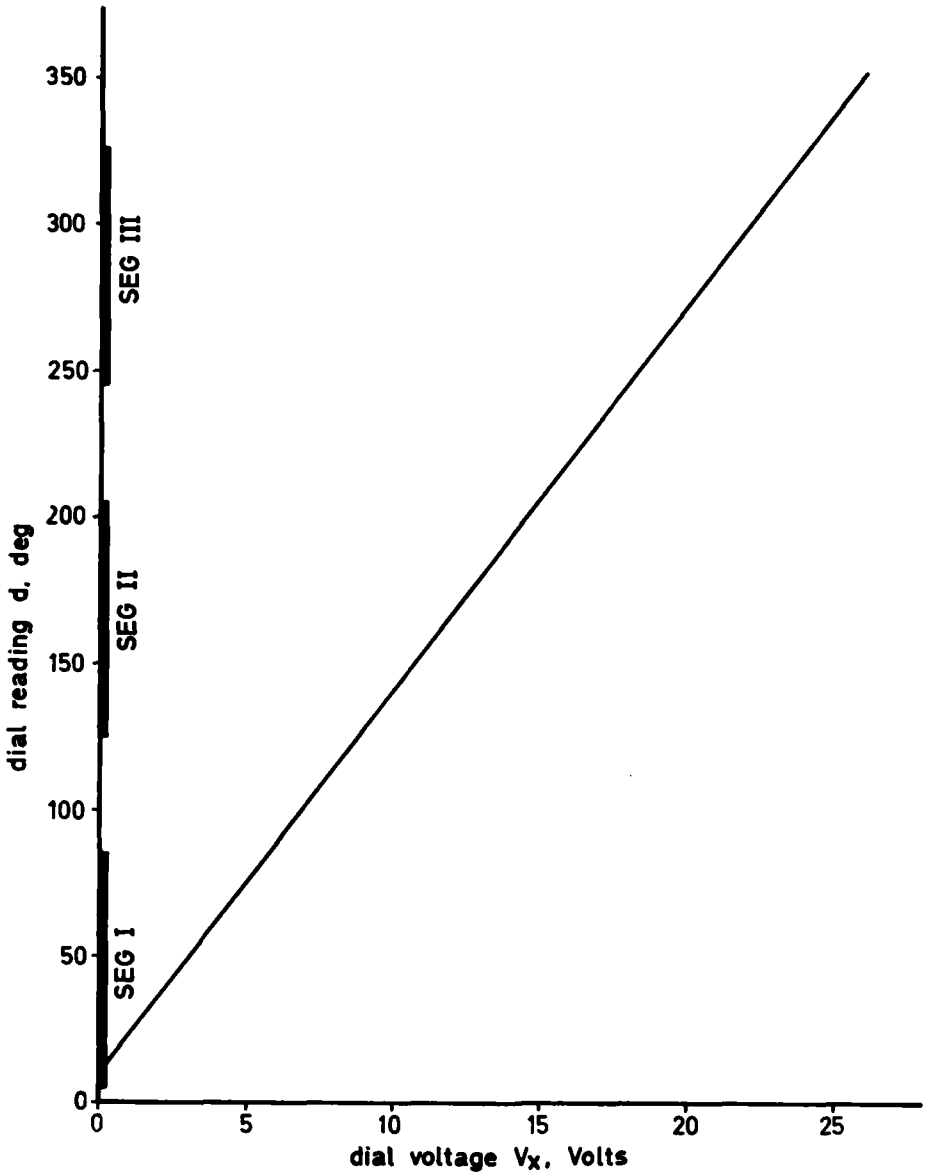

Figure 1. Measured relationship between dial reading and output voltage for the infrared filter wheel

$$d = 10.156 + 13.171\ V_x \qquad (V_x \text{ in volts, d in degrees}) \qquad (1)$$

This relationship holds only for positive V_x. The infrared filter turns on at $d = 6°$, whereas the related voltage remains zero until $d = 10°$. Hence, the small initial section of the spectrum cannot be measured, if V_x is used.

17. The infrared filter has three segments: SEG I, SEG II, and SEG III. Each segment is a narrow-band transmission filter in which the transmitted wavelength is a function of angular position θ. The parts of the filter wheel between the three segments are not transparent.

18. Data for the transmission characteristics of the segments are provided by the manufacturer (Optical Coating Laboratory, Inc. (OCLI), 2789 Griffen Avenue, Santa Barbara, Calif.) for seven values of angle θ wavelength λ for each segment. The transmission at other wavelengths is unknown, but we are assuming a smooth behaviour of the filter between measured points.

19. The three segments have been incorporated by Barnes into the filter wheel described above. However, the dial readings on the wheel differ from the angular positions θ of the segments. The first reason for suspecting such a difference comes from looking at the window in the filter wheel where the following clear and black sections are observed:

Dial Window in Filter Wheel			Detector Window in Filter Wheel	
Appearance	Dial From - to, deg	Width Δd	Dial From - to, deg	Filter Segment
Clear	185-265.5	80.5°	5-85.5	SEG I
Black	265.5-304.5	--	85.5-124.5	--
Clear	304.5-25	80.5°	124.5-205	SEG II
Black	25-65	--	205-245	--
Clear	65-164	81°	245-326	SEG III
Black	164-185	--	326-5	--

The detector window readings in the filter wheel are approximately 180° different from the dial window readings. This shifts the clear and black areas for the detector by approximately 180°. Thus, according to the dial, the transparent filter sections have widths Δd of approximately 80°, whereas the width of each section in terms of angle θ is $\Delta\theta \approx 90°$.

20. In calibrating the instrument, the relationship between θ and d has to be determined. The original calibration data from Barnes do not even mention this problem. The latest data from the manufacturer provide a formula which WES considers to be wrong.

Calibration of SEG II

21. This is treated first since it is the most straightforward. A number of water vapor absorption bands fall into this spectral region and can be used for calibration. Figure 2 shows two X-Y plots, one for manual rotations of the filter wheel and one for motor-driven rotations, which give detector voltage as a function of dial voltage V_x. Data are from the HgCdTe detector looking at a blackbody of 200° C at a distance of 5 m. The separation of the spectrum into three segments is obvious. The narrow absorption bands in SEG II can be seen only on the manual plot, which indicates that the automatic rotation of the filter wheel is too fast. This is also evident from horizontal lag between the two curves.

22. The absorption bands (transmission < 90 percent) expected for our situation; i.e., range 5 m, water vapor contents $\rho = 6 \cdot 10^{-6}$ g/cm^3; can be calculated from the LOWTRAN model (Wolfe and Zissis 1978) and are given in Figure 3 as a function of wavelength λ. The similarity with Figure 2 is obvious. The differences are due to variations in detector response, which will be treated later.

23. Easily identifiable extrema from SEG II, Figure 2, and Figure 3 are plotted against each other in Figure 4. They can be represented by the following linear equation ($\rho = 0.9995$):

$$\lambda = 0.6536 \cdot V_x - 1.6774 \qquad (\lambda \text{ in } \mu m,\ V_x \text{ in volts}) \qquad (2)$$

This equation relates the dial voltage V_x to the wavelength λ.

24. Data for the infrared filter have been provided by the manufacturer and are shown in Table 1. It lists wavelengths λ and corresponding angles θ for the three segments. In SEG II, we find the wavelength λ as a function of angle θ:

$$\lambda = 0.04468 \cdot \theta + 4.0763 \qquad (\lambda \text{ in } \mu m,\ \theta \text{ in degrees}) \qquad (3)$$

From Equations 2 and 3:

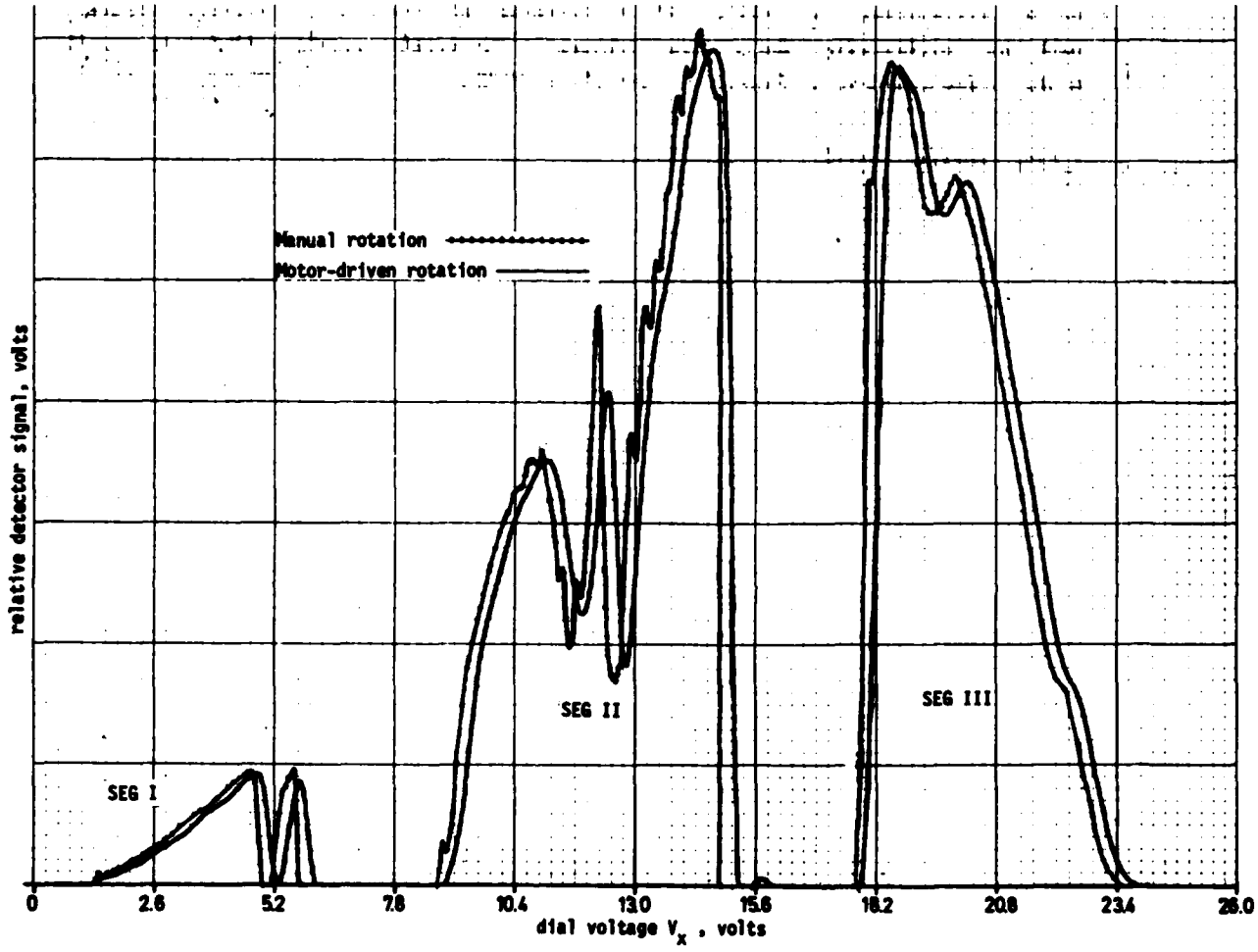

Figure 2. X-Y plots showing HgCdTe detector voltage as a function of dial voltage. Target is a blackbody of 200° C at a distance of 5 m. Vertical scale is 1 volt (V) per large division after 9 db attentuation

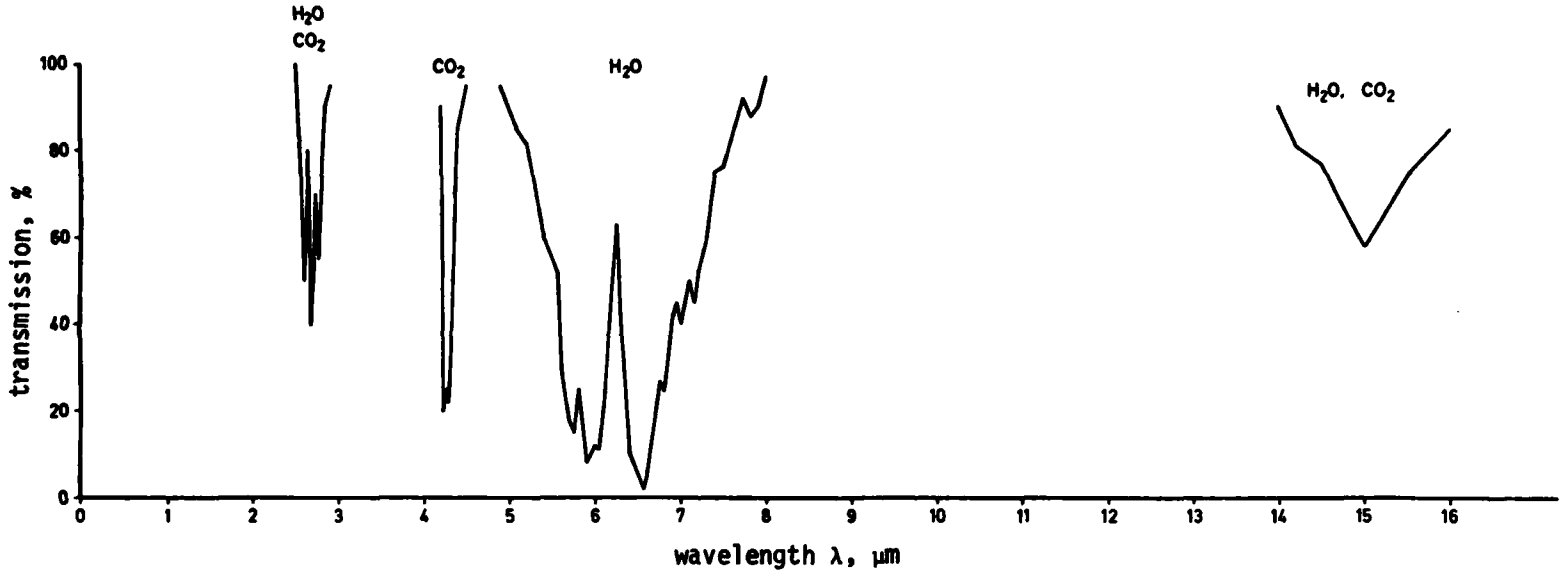

Figure 3. Absorption bands in air according to the LOWTRAN model

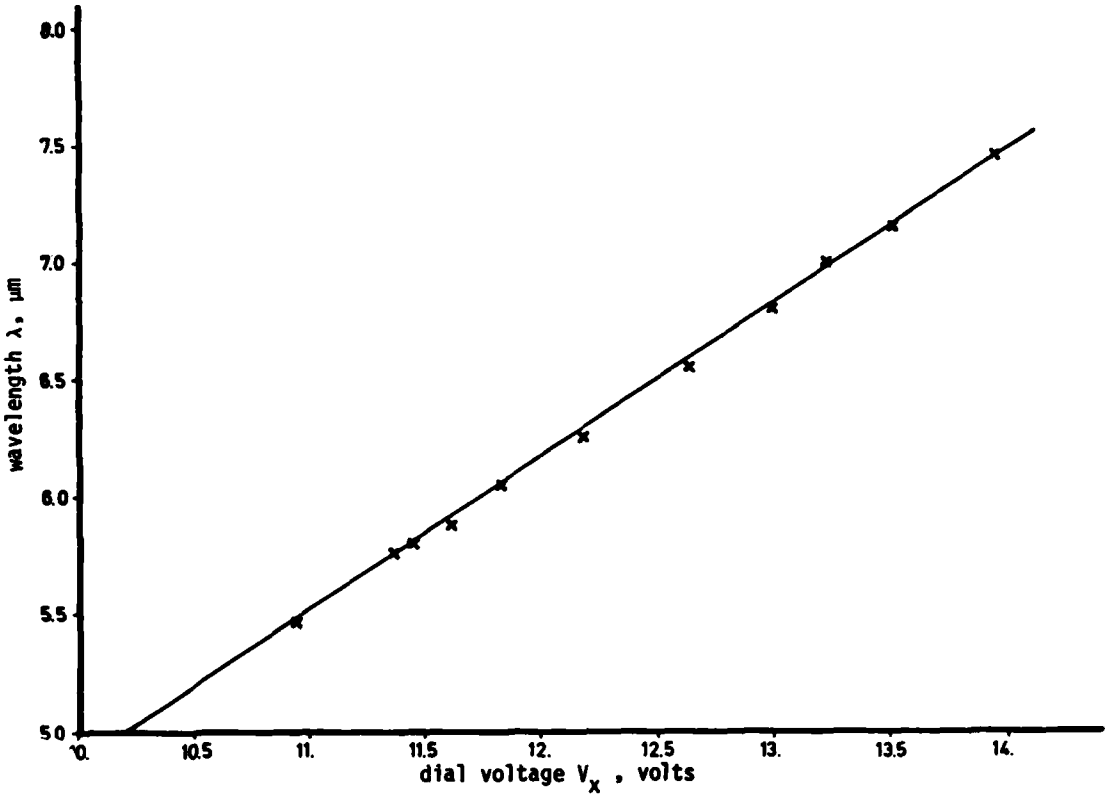

Figure 4. Calibration curve for wavelengths of infrared filter wheel

$$\theta = 14.628 \cdot V_x - 128.78 \qquad (\theta \text{ in degrees, } V_x \text{ in volts})$$

or with Equation 1

$$\theta = \frac{d - 126.103}{0.90037} \qquad (\theta \text{ and } d \text{ in degrees}) \qquad (4)$$

25. The beginning and end of SEG II are called cut-on and cutoff points. They were measured to be

cut-on: $d = 126.5°$ or $\theta = 0.44°$

cutoff: $d = 206.4°$ or $\theta = 89.2°$

This means the filter becomes transparent just after $\theta = 0°$ and opaque just before $\theta = 90°$.

Calibration of SEG I

26. Calibration of SEG I was done in analogy to SEG II. The InSb detector was pointed at a space heater at a distance of 10 m, and the positions of water vapor absorption bands at 2.6, 2.67, 2.77, and 3.20 μm and of a CO_2 band at 4.27 μm were recorded. The regression line of Equation 5 is obtained

$$\lambda = 2.44 + 0.36 \cdot V_x \qquad (\lambda \text{ in } \mu m,\ V_x \text{ in volts}) \tag{5}$$

From Table 1 we find

$$\lambda = 0.02386 \cdot \theta + 2.3663 \qquad (\lambda \text{ in } \mu m,\ \theta \text{ in degrees}) \tag{6}$$

with Equations 5 and 1

$$\theta = \frac{d - 7.38}{0.875} \tag{7}$$

Cut-on and cutoff points of SEG I are measured to be

cut-on: $d = 6°$ or $\theta = -1.6°$

cutoff: $d = 86.3°$ or $\theta = 90.2°$

Again, the filter segment is transparent approximately between $\theta = 0°$ and 90°.

Calibration of SEG III

27. No such convenient absorption bands are available in the 8- to 14-μm range of SEG III. The only absorption is found at 9.7 μm (V_x = 19.4 V) in measurements of sky radiation due to ozone. The filter cut-on can be determined as $V_x = 17.87$ and is taken as $\theta = 0$. In addition, we assume a slope of the θ-versus-d line of 0.88, similar to SEG's I and II. We obtain

$$\theta = \frac{d - 245.5}{0.88} \qquad (d \text{ and } \theta \text{ in degrees}) \tag{8}$$

28. Equations 4, 7, and 8 are plotted in Figure 5. The

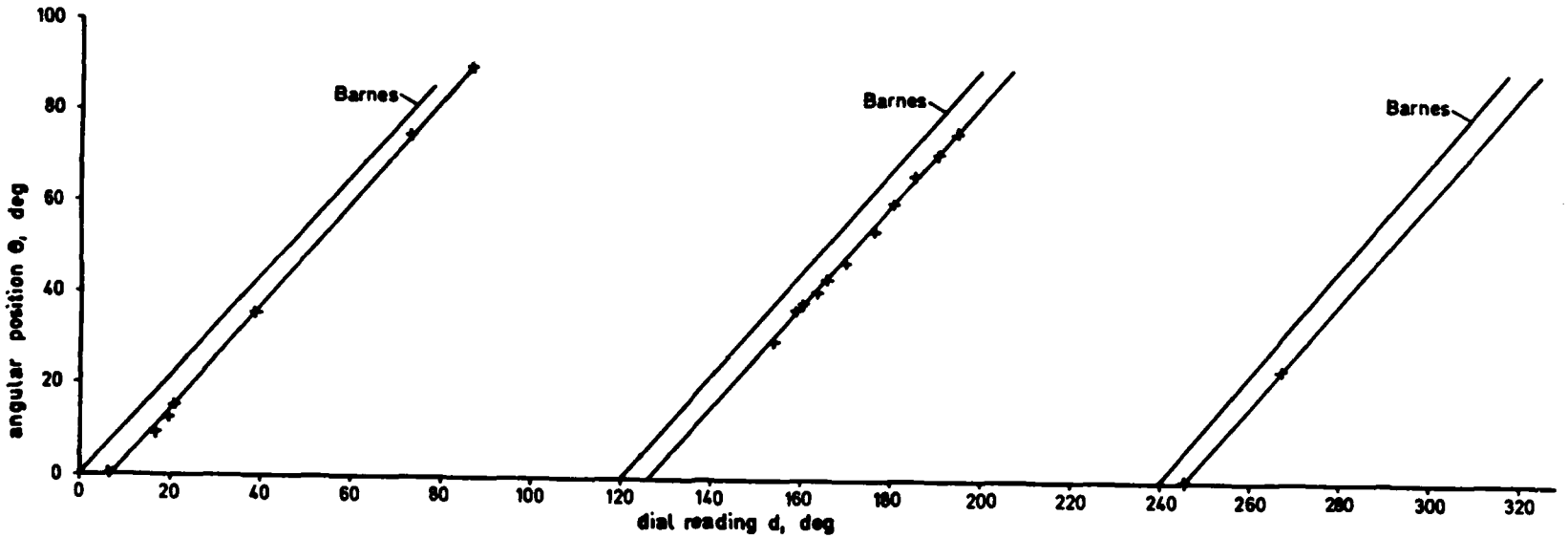

Figure 5. Relationship between angular position of filter segments and dial reading of infrared filter wheel. Crosses are measured points. The relationships provided by Barnes are shown for comparison

relationships provided by Barnes are shown for comparison. Our data differ basically because of a shift in the origin.

Visual and near infrared filter

29. The dial reading d of the filter wheel ($d = 0...360°$) can be monitored using the ramp voltage V_x . The linear relation between d and V_x is

$$d = 11.37 + 13.27\ V_x \qquad (V_x \text{ in volts, } d \text{ in degrees}) \qquad (9)$$

where V_x varies between 0 and 26 volts . The small initial section of the spectrum for $d < 11.4°$ cannot be measured using V_x . Equation 9 is almost the same as Equation 1 for the infrared filter.

30. The filter consists of two separate segments, SEG A (visual) and SEG B (near infrared), with a transition around 0.7 μm . Wavelength calibration proceeds in analogy to the infrared filter.

Calibration of SEG B

31. A measurement of the skylight just above the horizon shows distinct water vapor absorption bands at wavelengths of 0.69, 0.72, 0.76, 0.81, and 0.93 μm (Figure 6). A linear regression yields

$$\lambda = 0.0563V_x - 0.079 \qquad (V_x \text{ in volts, } \lambda \text{ in } \mu m) \qquad (10)$$

According to filter data (Table 2), wavelength and angular position of filter θ are related thus:

$$\lambda = 0.00454\theta + 0.6582 \qquad (\theta \text{ in degrees, } \lambda \text{ in } \mu m) \qquad (11)$$

From Equations 9, 10, and 11:

$$\lambda = 0.00424d + 0.127 \qquad (12)$$

and

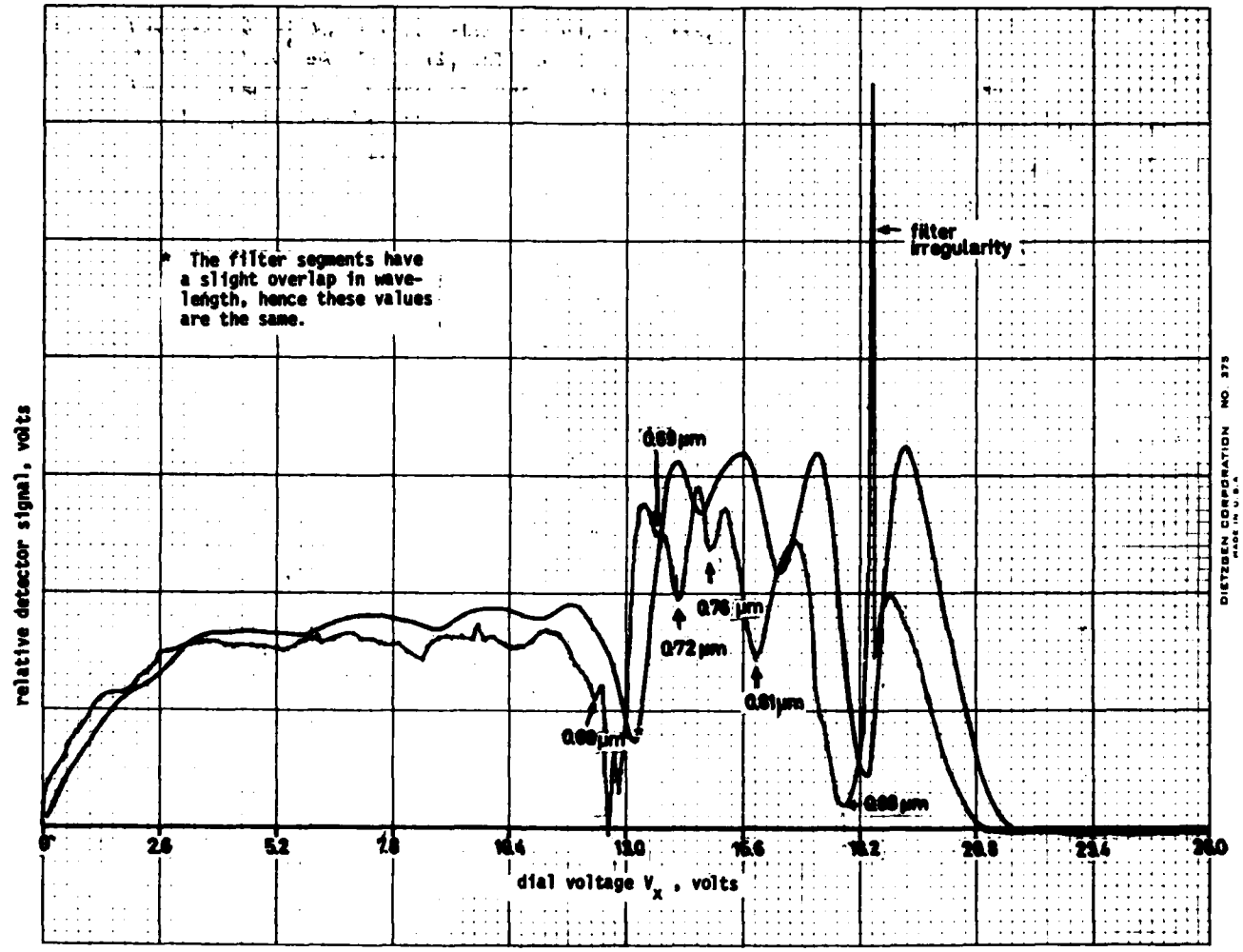

Figure 6. Radiance of the horizon sky in Vicksburg, Miss., looking west on April 13, 1981, at 1600 hours. Manual (dotted) and automatic traces are given. Wavelengths of absorption bands are indicated.

$$\theta = \frac{d - 182.9}{1.071} \qquad (13)$$

Calibration of SEG A

32. Since there is a slight overlap in wavelengths between SEG A and SEG B, the absorption band at 0.69 μm can also be observed in SEG A. In addition, extrema values from measurements of blue zenith sky and fresh green leaves were used as data points, yielding ultimately

$$\lambda = 0.024\ V_x + 0.395 \qquad (\lambda \text{ in } \mu m,\ V_x \text{ in volts}) \qquad (14)$$

or with Equation 9:

$$\lambda = 0.00181d + 0.374 \qquad (\lambda \text{ in } \mu m,\ d \text{ in degrees}) \qquad (15)$$

From Table 2

$$\lambda = 0.00197 \cdot \theta + 0.3631 \qquad (\lambda \text{ in } \mu m,\ \theta \text{ in degrees}) \qquad (16)$$

and with Equation 15

$$\theta = \frac{d + 6.13}{1.0875} \qquad (17)$$

Equations 1 through 17 have been tabulated in Table 3 for easy reference.

Automatic and manual recordings

33. The filter wheel can be rotated manually in small increments or it can be rotated continuously for automatic data collection. A full rotation takes about 20 sec for the visual and near infrared wheel and 40 sec for the infrared wheel. Unfortunately, both speeds are too fast for the detectors used. Consequently, automatic recordings are shifted in wavelength and show less spectral detail than manual recordings. All calculations so far were done for manual recordings. The shift can be taken into account approximately by adjusting the point of origin of the scan. If the target does not show much spectral variation,

automatic scanning can be used without losing information.

Radiation Concepts

34. The purpose of this section is not to describe the basic laws of radiation as they apply to the instrument (Wolfe and Zissir 1978, Barnes 1979). Instead, we will treat the instrument as a black box being defined by a transfer function between input and output. The input into this black box is radiation from the target, and the output is a voltage.

35. To simplify the relationships between input and output, consider a target whose radiation completely fills the field of view of the instrument. The parameter of the target to be measured is the spectral radiance n_t, which is a flux of energy per solid angle and per wavelength increment. It can be related to the output voltage U by

$$n_t = n_{ref} + \frac{U}{t} \qquad \left(\text{in} \quad \frac{W}{m^2 \Omega \mu m}\right) \tag{18}$$

where n_{ref} is the spectral radiance of the internal reference cavity (see paragraph 48) and t is the transfer function of the system, which describes the instrument and which we need to determine.

36. The transfer function $t(\lambda)$ can be rewritten as a wavelength-independent system response factor t_o/R_o times a wavelength-dependent relative response $R(\lambda)$:

$$t(\lambda) = \frac{t_o}{R_o} R(\lambda) = t_o \frac{R(\lambda)}{R_o} \tag{19}$$

In this equation t_o is the value of $t(\lambda)$ for $\lambda = \lambda_o$, and R_o is the value of $R(\lambda)$ for $\lambda = \lambda_o$; λ_o is a calibration wavelength to be chosen later. The reason for the factorization in Equation 19 is that we want to use the calibration data supplied with the instrument

as far as possible. The data do not provide $t(\lambda)$ or $R(\lambda)$, but only a normalized expression $R(\lambda)/R_o$. Knowing the wavelength dependence of this expression and measuring $t = t_o$ for one wavelength λ_o gives the transfer function t for all wavelengths through Equation 19.

37. The relative response $R(\lambda)$ is determined by two parts of the instrument, the response of the detector and the transmission of the filter for each wavelength. Accordingly, $R(\lambda)$ can be factored into

$$R(\lambda) = D(\lambda)\tau(\lambda) \tag{20}$$

with $D(\lambda)$ the relative detector response in percent as a function of wavelength and $\tau(\lambda)$ the transmission of the narrow band filter in percent per wavelength unit (usually μm).

38. The above equations have been derived for the case in which spectral radiance n_t is the radiation property to be measured. If instead an effective radiance is to be determined, the following analogous relationships apply. The expressions in Barnes (1977) are all given in terms of effective radiance, which is a flux of energy per solid angle. The effective radiance N_t is obtained from the spectral radiance n_t by integrating over a small wavelength interval $\Delta\lambda$:

$$N_t = \int n_t d\lambda \approx n_t \Delta\lambda \tag{21}$$

Calling the transfer function K, we have instead of Equation 18:

$$N_t = N_{ref} + \frac{U}{K} \tag{22}$$

with

$$K = \frac{t}{\Delta\lambda} = \frac{t_o}{R_o}\frac{R}{\Delta\lambda} = \frac{t_o}{R_o}\frac{D\tau}{\Delta\lambda}$$

Expressing the filter transmission τ as a peak transmission τ_p (in

percent) times the halfpower bandwidth $\Delta\lambda$(in μm)

$$\tau = \tau_p \Delta\lambda \tag{23}$$

we get for the transfer function K

$$K = \frac{t_o}{Ro} \; D\tau_p \tag{24}$$

39. In summarizing the last paragraphs, we have obtained two equally valid instrument transfer functions denoted t and K . For each transfer function, we have two equations

$$t = \frac{U}{n_t - n_{ref}} \left(\text{in} \; \frac{V}{W/m^2\mu m} \right), \; t = \frac{t_o}{R_o} \; D(\lambda)\tau(\lambda) \tag{25}$$

or

$$K = \frac{U}{N_\tau - N_{ref}} \left(\text{in} \; \frac{V}{W/m^2\Omega} \right), \; K = \frac{t_o}{R_o} \; D(\lambda)\tau_p(\lambda) \tag{26}$$

The left-hand equation describes the transfer function as output divided by input--both measurable quantities to some degree. The right-hand equation describes how the transfer function is composed of internal parameters. In the following sections, we will first determine the wavelength-dependent part of the transfer function, i.e., the relative response, and then the transfer function itself.

Determination of Relative Response

40. If radiation of a given wavelength is sensed by the radiometer, the output signal will depend upon the detector response and the filter transmission for the particular wavelength. We want to know the relative detector response and filter transmission for all wavelengths, which together give the relative response of the instrument. Relative response will be calculated separately for the infrared filter and for the visual and near infrared filter.

Infrared filter
wheel and HgCdTe detector

41. The relative response of the HgCdTe detector only has been measured by the manufacturer and is shown in Figure 7. Data are given in percent of maximum response, which occurs at a wavelength of $\lambda = 11$ μm .

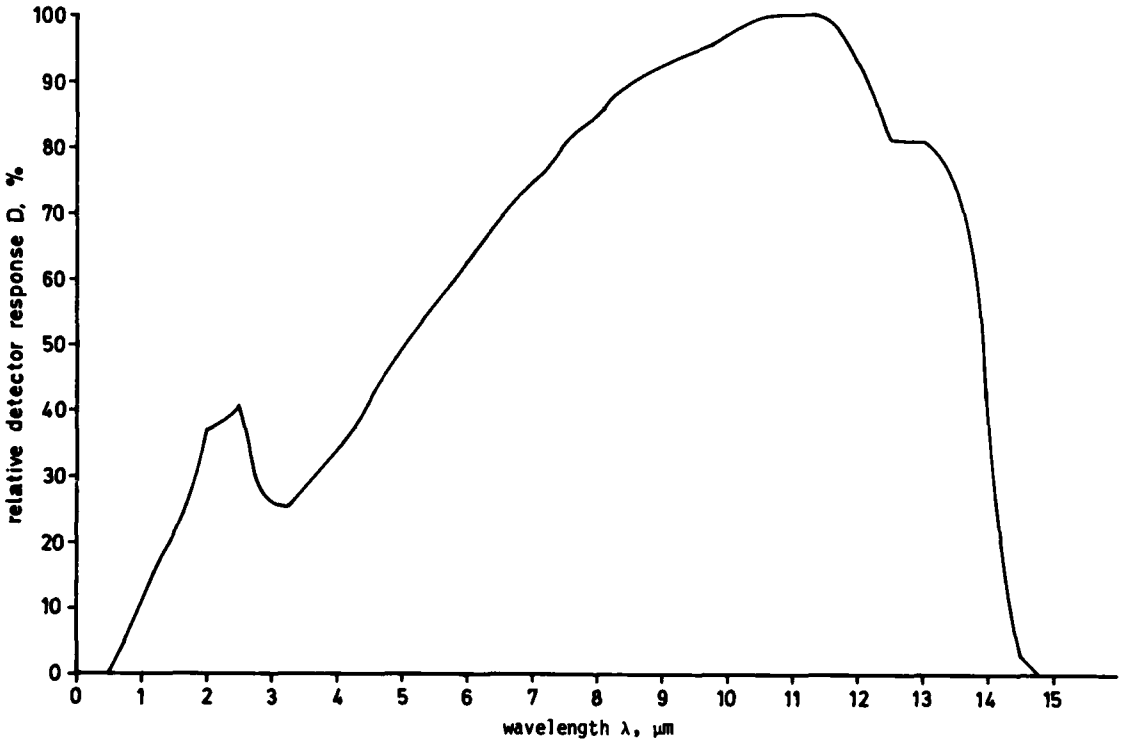

Figure 7. Response curve for HgCdTe detector

42. Data available for the filter wheel Segments I, II, and III are fairly limited. Narrow-band transmission curves (see Appendix B) are supplied for seven wavelengths in each segment. These are the wavelengths listed in Table 1. Transmission at other wavelengths is not known a priori, but a well-behaved filter should exhibit a smooth transmission curve between the measured points.

43. From the above data, filter transmission has been deduced in two ways. A triangular approximation gives the transmission as peak transmission multiplied by the half width of the narrow-band filter

(HBW from Table 2). In addition, the area under the filter curves has been measured planimetrically. Both ways resulted in columns A and B of Table 4. Except for two large discrepancies, the agreement between the methods is satisfactory. The discrepancies are obviously due to misprints in the data provided by the manufacturer. Column B will be used hereafter.

44. Relative response R is obtained by multiplying detector response D (Figure 7 and Table 4) by the filter transmission in column B of Table 4. The result is given in Table 4 in units of percent μm and in percent of the maximum value occurring at a wavelength $\lambda = 11.5$ μm. It is plotted in Figure 8. Comparison with Figure 7 shows that apart from irregularities at the edges of the filter segments, the relative response of detector-plus-filter follows the response curve for detector only.

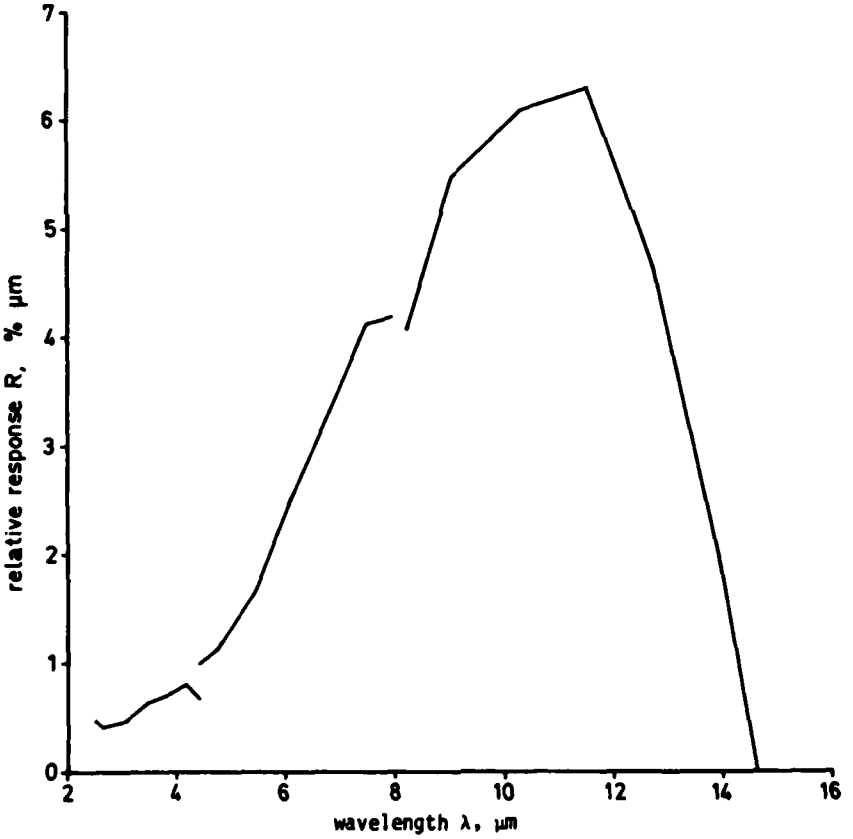

Figure 8. Relative response R of infrared filter and HgCdTe detector

Visual and near infrared
filter wheel and Si detector

45. Relative response $D(\lambda)$ of the silicon detector has been measured by Barnes, see Figure 9. Data for the filter transmission

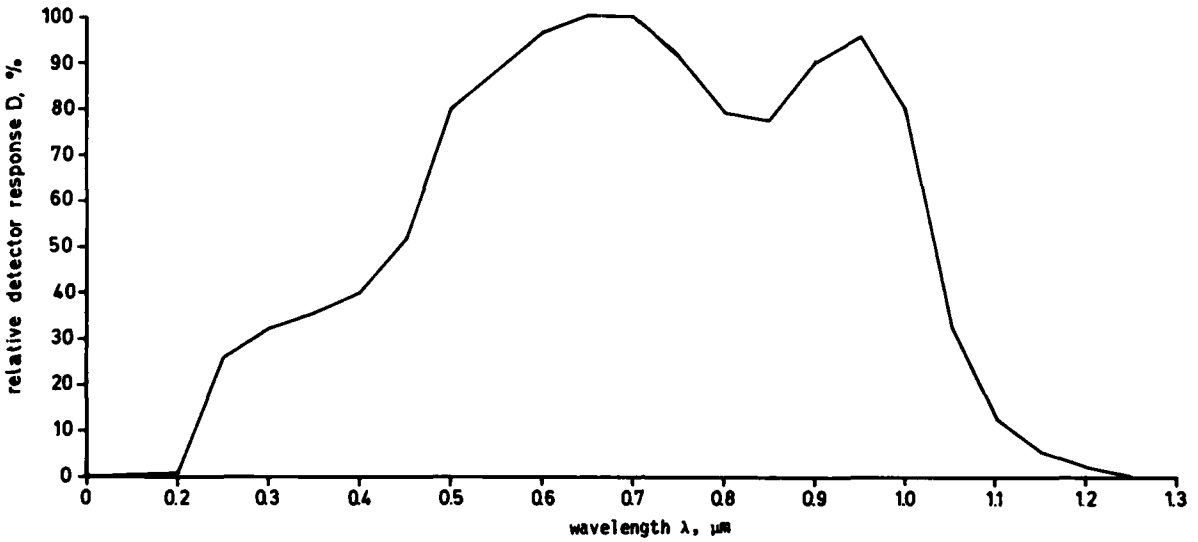

Figure 9. Response curve of Si detector

SEG A and SEG B are again limited to those wavelengths listed in Table 2; i.e., 13 wavelengths for each segment. Transmission curves for the wavelengths are included in Appendix B. From these curves, filter transmission τ was determined planimetrically. Results are shown in Table 5. Filter transmission τ and detector response D are multiplied to obtain the relative response R. R has been plotted in Figure 10 as a function of wavelength. It is not a very smooth function of λ in the near infrared, which poses a problem for interpolating between the calculated points. Figure 10 shows the simplest relationship, which is a linear interpolation, but any other interpolation could be used as well. In addition, an anomalously high response occurs at $\lambda = 0.97$ µm. It can be seen in the measurements of Figure 6 and is obviously due to a damage spot in the filter wheel.

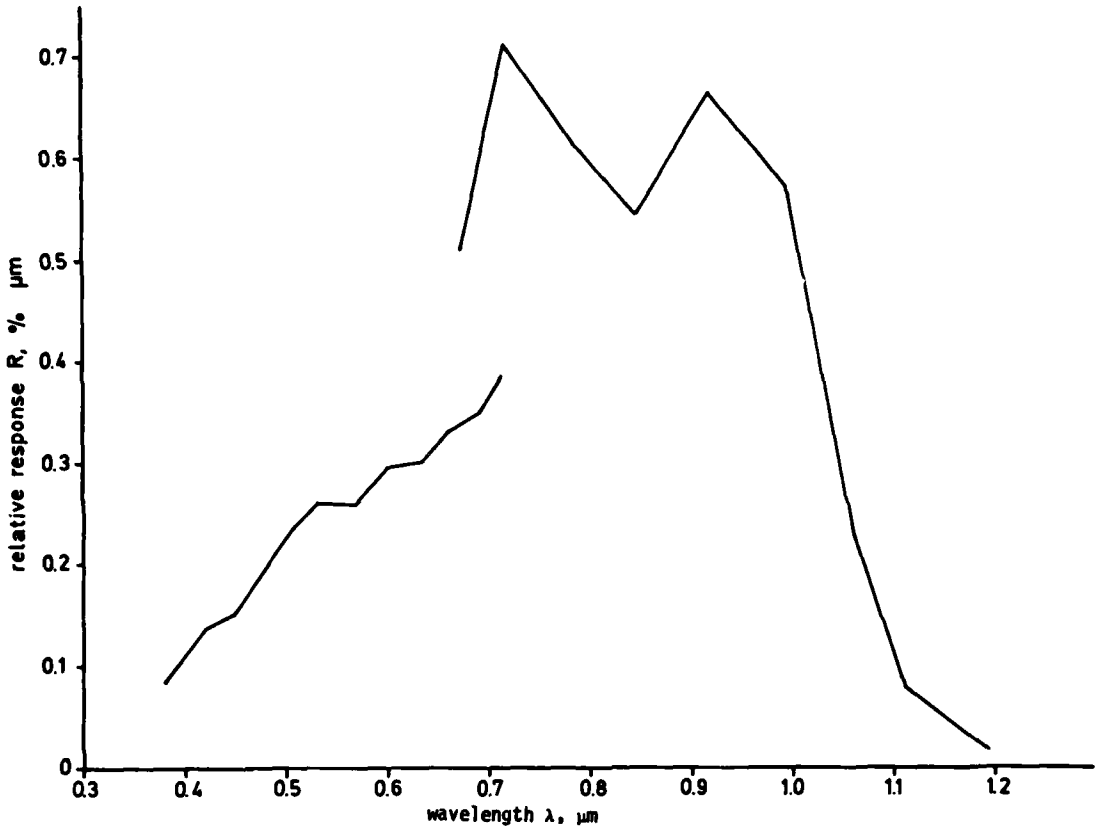

Figure 10. Relative response R of visual and near infrared filter and Si detector

Blackbody Source

46. To measure the transfer function of the SpectralMaster instrument, a source with known radiation is needed. A suitable source is a so-called "blackbody" with variable temperature. The temperature can be measured with a thermocouple, and the spectral radiance can be calculated from the temperature using Planck's radiation law.

47. A Barnes Model 11-101 radiation source was available. It has an aperture diameter of 16 mm and a built-in thermocouple to monitor core temperature. The temperature can be varied between ambient and 230° C. The manufacturer claimed the thermocouple to be a Pt-Pt/13 percent Rh thermocouple. The voltage-temperature characteristic expected from such a thermocouple is shown as the upper curve of Figure 11.

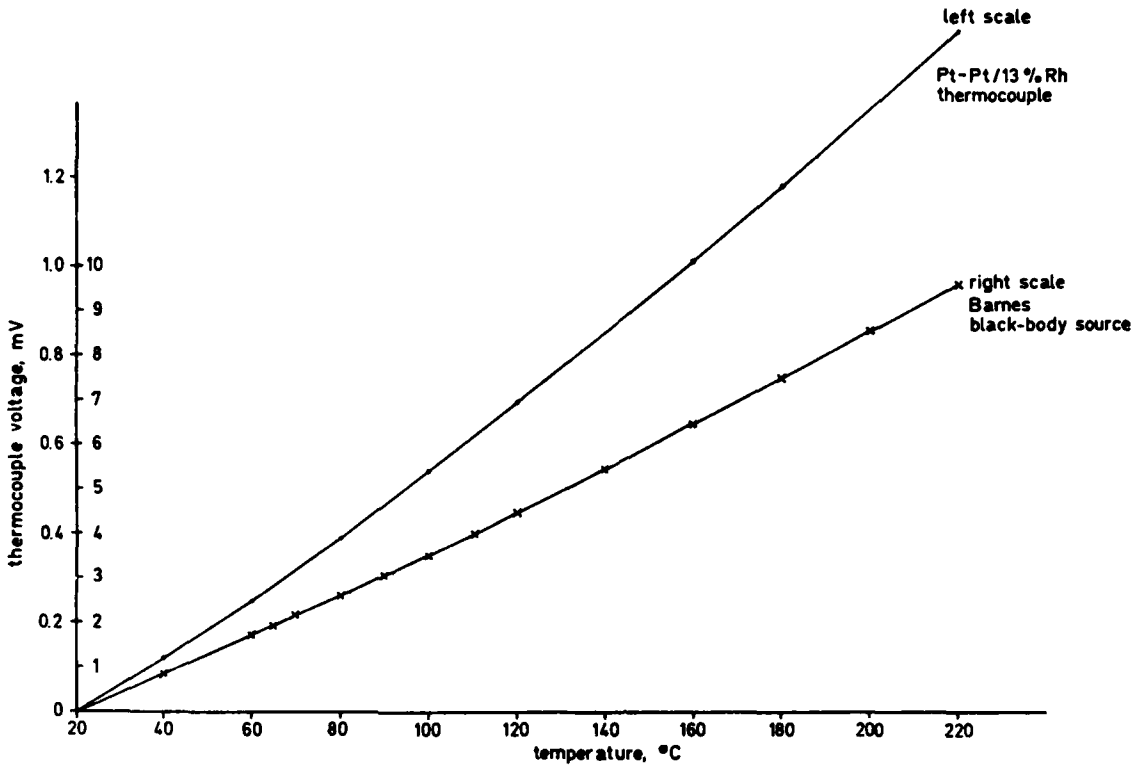

Figure 11. Characteristics of two different thermocouples. Measured points (crosses) of the Barnes blackbody source agree with the temperature characteristic of a copper-Constantan thermocouple (bottom curve)

Measuring the characteristic of the installed thermocouple, we obtain the crosses on the bottom curve. This curve is very different, but agrees well with the characteristic for a Cu-Constantan thermocouple. It will be used hereafter.

Effective Temperature of Reference Cavity

48. Equation 25 (see paragraph 39) for the transfer function t

$$t = \frac{U}{n_t - n_{ref}} \qquad (25 \text{ bis})$$

shows that the input for the system is $n_t - n_{ref}$; i.e., the difference between the spectral radiance of the target n_t and of the internal reference cavity n_{ref} . The transfer function can be determined only when the reference radiance n_{ref} is known.

49. The reference cavity is held at a nominal temperature of 50° C. However, some of the walls of the cavity are highly reflecting and the cavity cannot be considered a good blackbody. We want to determine the effective radiation temperature of the cavity experimentally. This can be done by pointing the radiometer at the blackbody source and varying the temperature of the blackbody until a null signal is obtained. The reference temperature is then equal to the blackbody temperature. However, the distances from blackbody to detector and from reference cavity to detector are not the same, so the above comparison must be limited to wavelengths for which the difference in atmospheric absorption over the two distances is negligible.

50. Figure 12 shows detector voltage versus wavelength for a number of different black body temperatures. For the blackbody at room temperature, we obtain a fairly smooth curve without any absorption bands. This is because any radiation absorbed in the pathlength will be reemitted the same way. With increasing source temperature, the absorption bands become more and more pronounced. For target temperatures below that of the reference cavity, the observed signal is negative. Figure 12 indicates that the reference temperature is expected to be between 50° and 70° C.

51. A closer look at the reference temperature is provided by Figure 13, where the source temperature has been varied in smaller increments between 58° and 65° C. For wavelengths with negligible absorption in air, a null signal is obtained whenever source temperature and effective reference temperature coincide (see the arrows in Figure 13). Unfortunately, the effective reference temperature is not constant, but varies between 60° and 65° C depending on wavelength. In the following, we use a reference temperature of 60° C for SEG II, because it corresponds to the large absorption-free part around 5 μm,

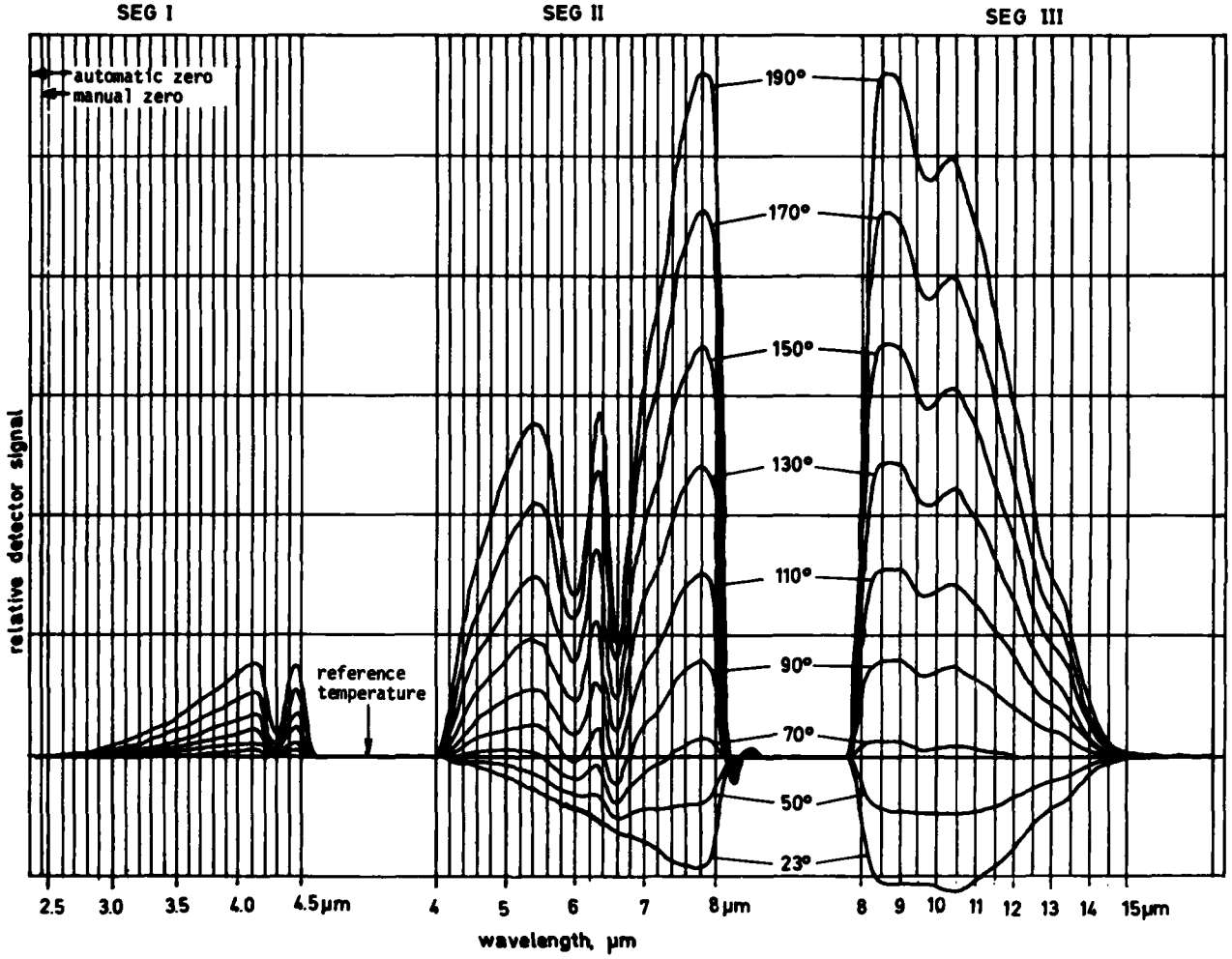

Figure 12. Signals observed with the HgCdTe detector from a blackbody at temperatures between 23° C and 190° C. Vertical scale was 1 V per large division after 9 db attenuation. Distance between blackbody and detector was 3 m

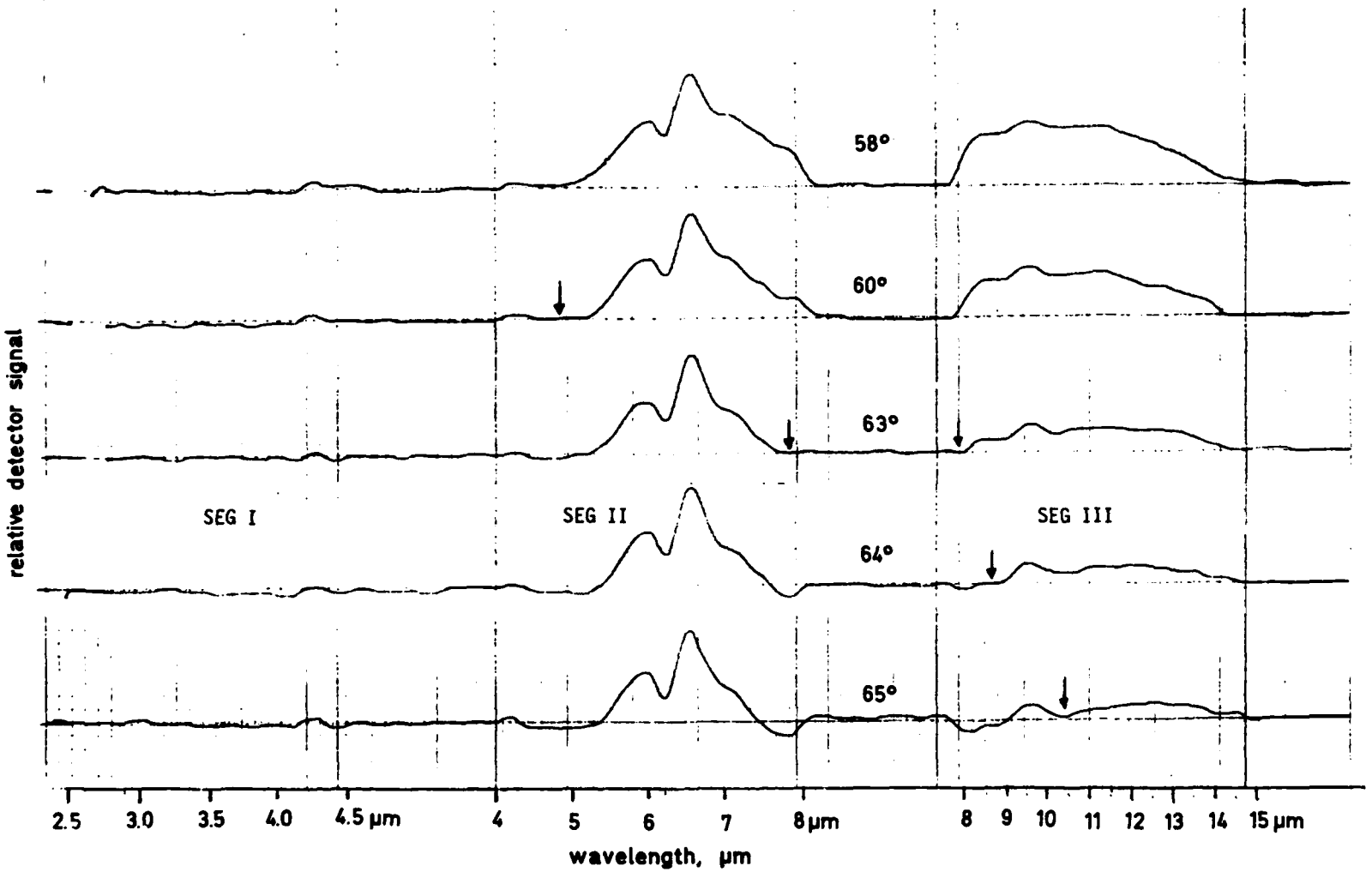

Figure 13. Signals observed with the HgCdTe detector from a blackbody at temperatures between 58° C and 65° C. Arrows indicate null signal

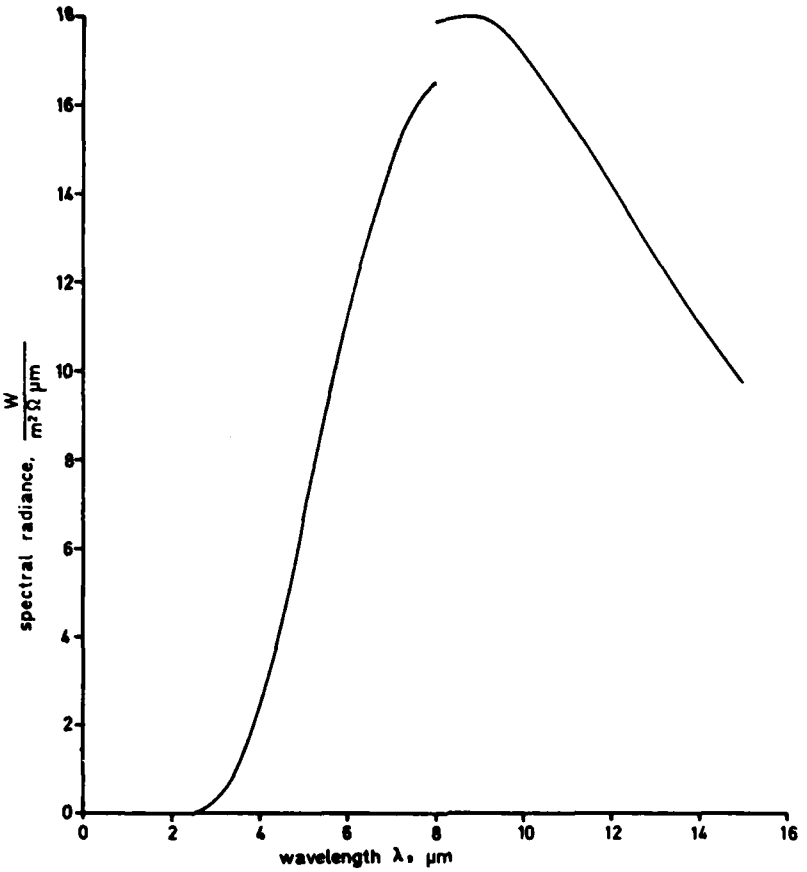

Figure 14. Spectral radiance n_{ref} of reference cavity

and of 65° for SEG III because it describes best the whole fairly absorption-free segment. Signals in SEG I are too weak to determine the reference temperature with the null method. It will be taken as 60°.

52. Once the effective temperature of the reference cavity was known, the spectral radiance of the cavity n_{ref} was calculated from Planck's radiation law. Results for the wavelengths of interest are plotted in Figure 14. The gap at $\lambda = 8$ μm occurs because of the assumed change of effective cavity temperature.

Determination of the Transfer Function

53. The transfer function t was measured only for the instrument equipped with the infrared filter. The high-temperature source

necessary to determine the transfer function in the visible was not available. The radiometer will be used in the visible; but it will be used primarily to measure relative values, hence a knowledge of the absolute value of t is not necessary.

54. The instrument was pointed at a blackbody source of temperature t_s and the resulting signal voltage U measured. Spectral radiances n_s and n_{ref} were calculated from the known temperatures t_s and t_{ref}. The transfer function t was obtained from

$$t(\lambda) = \frac{U}{n_s(\lambda,t_s) - n_{ref}(\lambda,t_{ref})} \qquad (27)$$

Results are presented in Table 6 for source temperatures of 25°, 100°, 180°, 200° C, and for wavelengths with negligible absorption in air. When source temperature is equal to room temperature (25° C), wavelengths with significant absorption can also be used. However, signals from room-temperature sources in filter segment SEG I are too weak to be useful. Signals at the long wavelength limit are also quite weak; this eliminates $\lambda = 14.59$ μm and casts doubts on the values for $\lambda = 13.88$ μm.

55. According to its definition, the system transfer function t should be independent of source temperature. The results for t in Table 6 show indeed little dependence on temperature.

56. Another way of interpreting the data is by taking the ratio of t and R, which is the system response factor. This number should be independent of both source temperature and wavelength. Results for the system response factor have been included in Table 6. While all numbers are of the same order of magnitude, there is considerable variation within the columns of the table; i.e., among different wavelengths. Variations within the rows; i.e. among different temperatures; are less pronounced.

57. As will be seen later, for most practical measurements the use of the transfer function can be avoided. If not, t is required for data evaluation as a function of wavelength. Two procedures are proposed (see Figure 15):

a. One method is to disregard the data for relative response and to rely on the measured transfer function. In this case a suitable average of t over different temperatures is used such as given in Table 6, column 6. This results in the crosses in Figure 15.

b. The other method is to rely on the data for relative response and to use the measurements of transfer function only to convert the relative response into an absolute response. From Table 6, an average value for for the system response factor of 7.1 $Vm^2\Omega/W$ can be derived by averaging all the system response factors for Segments II and III except for the suspect values at 13.8816. Segment I values are not included because of the weakness of the signals discussed previously in paragraph 54. The transfer function t is then

$$t = 7.1 \frac{Vm^2\Omega}{W} R(\lambda) \qquad (28)$$

The results are shown in Figure 15 as connected dots.

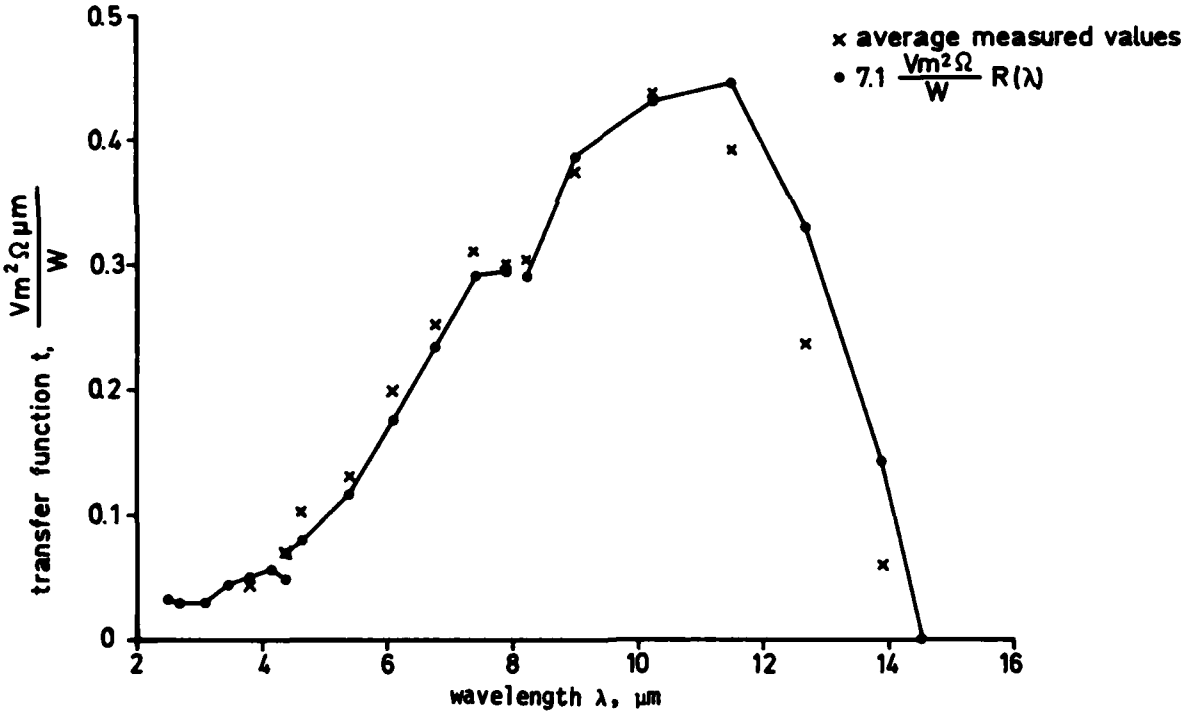

Figure 15. Infrared transfer function calculated in two different ways; crosses show results for Method a, connected dots for Method b

The difference between results for both procedures is not large. However, the second method is recommended since measured t values are not available for all wavelengths.

58. In summary, Part II has provided the theoretical background for understanding the Barnes SpectralMaster; equations have been derived for interpreting the signal voltages of the instrument. Part III describes how this applies to the measurement of surface parameters.

PART III: MEASUREMENT PROCEDURE

59. In the following we shall consider only spectral measurements; i.e., measurements where the wavelength dependence of a parameter is to be determined. For integrated measurements, say for $\lambda = 8$ to 14 μm, simpler radiometers can be used as well.

60. For spectral measurements, the detector voltage has to be recorded as a function of the rotation of the filter wheel. It is most convenient to use an X-Y plotter for this purpose, with the detector voltage as V_y and the dial voltage as V_x. The relationship between V_x and wavelength λ has been determined in Part I (see Table 3). The relationship is stepwise linear and can be used to design a graph paper for the X-Y plotter so that the X-axis reads directly in wavelength. Examples are provided in Appendix C. The two papers shown require that the full scale of $V_x = 26$ V corresponds to 10 in. on the X-axis of the paper. The graph papers were designed for manual rotation of the filter wheel. Automatic rotation of the filter wheel is too fast for the detector response and produces a time lag in the output signal. The time lag can approximately be compensated for by starting the trace on the "automatic zero" line of the graph paper.

61. Three types of measurements will be discussed: reflectance, radiance, and emissivity.

Reflectance

62. Reflectance describes how much radiation is reflected from a given target as compared to the amount reflected from standard surface when both are illuminated by a light source (often the sun). The standard should be a highly reflecting Lambertian (i.e., diffusely reflecting) surface.

63. Two measurements for each wavelength are required, one for the target and one for the standard. They result in the signal voltage U_t for the target and U_{stand} for the standard. From Equation 18, the spectral radiances received by the radiometer are determined to be

$$n_t = n_{ref} + \frac{U_t}{t} \approx \frac{U_t}{t} \quad \text{for the target} \tag{29}$$

$$n_{stand} = n_{ref} + \frac{U_{stand}}{t} \approx \frac{U_{stand}}{t} \quad \text{for the standard} \tag{30}$$

The small contribution n_{ref} from the internal reference cavity can be neglected for measurements in the visible and near infrared. The reflectance R is then

$$R = \frac{n_t}{n_{stand}} \tag{31}$$

and with Equations 29 and 30

$$R = \frac{U_t}{U_{stand}} \tag{32}$$

64. Thus, measuring reflectance does not require a knowledge of the system transfer function t. All that is needed is the ratio of two output voltages for each wavelength. The accuracy of the measurements will clearly depend to a large degree on the quality of the standard surface used.

65. If the bidirectional reflectance is to be measured, all of the above comments apply. Simply repeat the reflectance measurement for a large number of different angles of incident and reflected light.

Radiance

66. Determining radiance requires an absolute measurement and, therefore, a knowledge of the system transfer function. It can be done in several slightly different ways.

Use of Barnes instruction manual

67. According to Barnes (1977, 1979), effective radiance N_t in watts/cm$^2\Omega$ is obtained from

$$N_t = N_{ref} + \frac{U_t}{K_s} \tag{33}$$

We assume (a) the simplest case of the target filling the field of view and (b) that the attenuation factor and the Electronic Temperature Offset (ETO) have been properly considered to obtain the signal voltage U_t. The system response factor K_s and the reference radiance N_{ref} are given in the calibration manual for one wavelength in each filter segment. For other wavelengths, K_s has to be multiplied by a number obtained from the curves for "relative response." These relative response curves must be considered as fairly crude approximations; replacing them with a suitably chosen straight line might work as well. What to do for N_{ref} at other wavelengths remains obscure. Hopefully, the variations in N_{ref} are so small that it makes no difference. This procedure is not recommended.

Use of this report

68. If infrared radiance is to be determined, results from Part II provide a better data base. Whereas the data in Barnes (1977) are given in effective radiance ($W/cm^2\Omega$), the data in this report refer primarily to spectral radiance ($W/cm^2\Omega\ \mu m$). Spectral radiance n_t is measured as

$$n_t = n_{ref} + \frac{U_t}{t} \tag{34}$$

The reference radiance n_{ref} can be calculated for all wavelengths from Planck's radiation law, or it can be taken from Figure 14. The system transfer function t can be written as a system response factor t_o/R_o times a relative response $R(\lambda)$:

$$t = \frac{t_o}{R_o} R(\lambda) \tag{35}$$

From Table 6, we find an average value for the system response factor of

$$\frac{t_o}{R_o} = 7.1\ \frac{Vm^2\Omega}{W} \tag{36}$$

$R(\lambda)$ has been calculated for 21 wavelengths in Table 4. The values at other wavelengths have to be obtained by interpolation.

69. For example, for $\lambda = 11.5$ μm, we find $R = 6.30\%$ μm from Table 4 and

$$t = \frac{t_o}{R_o} \quad , \quad R = 7.1 \ \frac{Vm^2\Omega}{W} \quad , \quad 6.30\% \ \mu m = 0.45 \ \frac{Vm^2\Omega\mu m}{W}$$

From Figure 14, $n_{ref} = 15 \ W/m^2\Omega \ \mu m$, and

$$n_t = \left(15 + \frac{U_t}{0.45V}\right) \ \frac{W}{m^2\Omega\mu m} \qquad \text{(for } \lambda = 11.5 \ \mu m\text{)}$$

Use of a blackbody source

70. If a blackbody source is available, it can be used to obtain a more accurate value for the system response factor than Equation 36. It will also eliminate any changes in detector sensitivity that might have occurred. To reduce inaccuracies, the blackbody temperature should be significantly different from the temperature of the reference cavity, say 200° C, for measurements in the infrared. To determine radiance in the visual and near infrared, blackbody temperature has to be at least 2000° C.

71. The system response factor t_o/R_o can be calculated from measuring the radiance n_{BB} of the blackbody source

$$\frac{t_o}{R_o} = \frac{U_{BB}}{(n_{BB} - n_{ref})R} \qquad (37)$$

U_{BB} will be measured, R is from Table 4 or 5, n_{BB} and n_{ref} are calculated from Planck's equation when the temperature of the blackbody and of the reference are known. Measurements should be made at a wavelength suffering negligible absorption in air, such as

SEG I: $\lambda = 3.8\ \mu m$ ($V_x = 3.79$ volts)
SEG II: $\lambda = 5.4\ \mu m$ ($V_x = 10.82$ volts) for InSb detector
SEG III: $\lambda = 11.5\ \mu m$ ($V_x = 20.91$ volts) for HgCdTe detector

For the Si detector, all wavelengths can be used.

Use of room temperature radiation

72. If the radiometer is operated in a closed room at a homogeneous temperature, the room will be a good approximation to a blackbody and a radiance measurement yields n_{BB}. If the radiometer is operated outdoors, the closed room can be simulated simply by putting the cap on the radiometer.

73. Combining Equations 34 and 37 to eliminate t we get

$$\frac{n_t - n_{ref}}{n_{BB} - n_{ref}} = \frac{U_t}{U_{BB}}$$

or

$$n_t = n_{ref} + (n_{BB} - n_{ref}) \frac{U_t}{U_{BB}} \qquad (38)$$

U_t and U_{BB} are measured, n_{ref} and n_{BB} can be calculated from Planck's equation. The advantage of Equation 38 is that R is not required since Equation 38 can be used for all wavelengths; at room temperature, absorption in air plays no role. In contrast to all previous methods, no extrapolation to other nonmeasurable wavelengths is necessary. The disadvantage of Equation 38 is that the temperatures of the reference cavity and of the blackbody differ by only about 40° C. It means that the radiance difference in Equation 38 becomes small, which increases the uncertainty of the measurement.

Emissivity

74. Determining target emissivity is of interest only in the

infrared region. Radiance received by the radiometer from any target consists of emitted radiation and reflected background radiation. For opaque targets, reflectivity r plus emissivity ε equal 1: $r + \varepsilon = 1$. Then

$$n_t = \varepsilon n_{BB}(T) + (1 - \varepsilon)g_B \tag{39}$$

where $n_{BB}(T)$ is the blackbody radiance of the target at temperature T and g_B the irradiance from the background (Richmond 1980).

75. To determine ε from Equation 39, it is necessary to vary either the background radiation or the target temperature. The first method is useful for in situ measurements, where the target temperature cannot be influenced (Buettner and Kern 1965). The second method is good for targets which can be heated in the laboratory.

Field measurements of emissivity

76. Assume a horizontal target exposed to the radiation from a clear sky without direct solar radiation. Obstructions of the sky should be minimized. Radiance from the target n_t is measured:

$$n_t = \varepsilon n_{BB} + (1 - \varepsilon)g_{sky} \tag{40}$$

After enclosing the target and the radiometer in a "black box" or suitable shroud, the radiance of the target is measured again. The value obtained is equal to n_{BB} in Equation 40. The surface temperature of the target should not change between both measurements--that is why direct solar radiation should be avoided. In a third measurement, we have to determine the hemispherical sky radiation. This can be done by measuring the radiance at various zenith angles and integrating over the hemisphere. However, the radiation from a clear sky is so diffuse that the hemispherical irradiance can be replaced by the sky radiance measured when pointing the radiometer vertically upward (Lorenz 1966). Rearranging Equation 40 we get

$$\varepsilon = \frac{n_t - n_{sky}}{n_{BB} - n_{sky}} \tag{41}$$

Substituting the radiometer equation

$$n = n_{ref} + \frac{U}{t}$$

in Equation 40 gives

$$\varepsilon = \frac{U_t - U_{sky}}{U_{BB} - U_{sky}} \tag{42}$$

with n_{ref} and t being eliminated. U_t is the signal voltage from the exposed target, U_{BB} from the enclosed target, and U_{sky} the signal voltage from the zenith sky.

Laboratory measurement of emissivity

77. We need the target and a standard of known emissivity. Both will be measured at room temperature T_1 and at an elevated temperature T_2 (Richter 1980). Radiance from the target T_2 (emissivity ε_t) is

$$n_2(T_2) = \varepsilon_t n_{BB}(T_2) + (1 - \varepsilon_t)n(T_1) \tag{43}$$

and from the standard (emissivity ε_{stand}) at the same temperature T_2

$$n_{stand}(T_2) = \varepsilon_{stand} n_{BB}(T_2) + (1 - \varepsilon_{stand})n(T_1) \tag{44}$$

where $n_{BB}(T_2)$ is the radiation of a blackbody at temperature T_2 and $n(T_1)$ the background radiation. If the target and the standard are at room temperature T_1, Equations 43 and 44 reduce to

$$n_t(T_1) = n(T_1) = n_{stand}(T_1)$$

Hence the background radiation is obtained by measuring the radiance of either the target or the standard at room temperature. Eliminating $n_{BB}(T_2)$ from Equations 43 and 44 and rearranging, we obtain

$$\frac{\varepsilon_t}{\varepsilon_{stand}} = \frac{n_t(T_2) - n(T_1)}{n_{stand}(T_2) - n(T_1)} \tag{45}$$

Equation 45 is very similar to Equation 41, and we can replace the radiances by the signal voltages:

$$\frac{e_t}{\varepsilon_{stand}} = \frac{U_t - U_o}{U_{stand} - U_o} \tag{46}$$

where U_t is the signal voltage from the heated target, U_{stand} from the heated standard of known ε_{stand}, and U_o the signal voltage from unheated objects in the closed laboratory.

78. It should be emphasized that the target and the standard have to be at the same temperature. This means a blackbody source as described in paragraph 70 cannot be used as a standard. Instead, the standard must be a section of the target surface which has been painted with a black paint of known emissivity.

PART IV: SPECTRAL CHARACTERISTICS OF DESERT SURFACES

79. Different types of desertic sand and rock occurring in the vicinity of Moab, Utah, have been collected. Their reflectance properties in the visible and near infrared and their emissivity in the thermal infrared have been measured. The results provide examples of measurements possible with the Barnes SpectralMaster radiometer.

Materials Measured

80. Two types of sand were measured: a red silty sand of sandstone origin from Sand Flats and a grey sand of shale origin (sandy clay) from Klondike Flats, both near Moab. Mineralogical analysis was as follows:

	Contents in Weight, %							
Origin	Al_2O_3	CaO	Fe_2O_3	K_2O	MgO	Na_2O	SiO_2	Total
Sand Flats	2.83	0.21	2.67	1.46	0.08	0.23	92.72	100.2
Klondike Flats	12.07	3.43	0.34	2.70	0.46	0.43	67.22	86.7

81. The red sand had a mean grain size diameter of 0.15 mm, with a narrow, normal distribution. The red color was due to the high Fe_2O_3 content. The grey sand had a mean grain size diameter of 0.04 mm. The distribution was not normal, with many very small grains. The mineralogical analysis did not tally up to 100 percent, indicating contents of organic matter. Humidity in both samples was negligible.

82. In addition, a slab of red sandstone, the rock from which the red sand above derives, was measured. Parts of the exposed rock surfaces were covered with red and black lichens, which were measured, too.

Measurement Technique

83. Emissivity for wavelengths from 3 to 14 μm and reflectance for wavelengths from 0.4 to 1.1 μm were measured with the Barnes SpectralMaster Radiometer Model 12-550.

84. Reflectance was measured in situ on a completely cloudfree day, with the sun around noontime as radiation source. Radiation reflected from the targets was compared with that from a panel coated with Eastman White Reflectance Coating. This is a barium sulfate based coating with a nominal reflectance in the visible of 0.99 for angles of incidence and reflectance of less than 30° from the surface normal. During the reflectance measurements, the radiometer was focused at infinity, implying a measured area 10 cm in diameter and a radiation-collecting angle of 2.5 mrad.

85. A typical X-Y plot obtained for such a reflectance measurement is reproduced in Appendix C, Figure C3. It shows one trace for the white standard and four very similar traces for the red sand under different azimuth angles. There is a large dip in the middle of the graph which is due to an opaque section of the filter wheel. At a wavelength of 0.97 μm, the trace goes off scale which indicates a damage spot in the filter. Both extremes contain no information about the target to be measured. To obtain reflectance, the amplitude of the target signal has to be divided by the amplitude of the white standard. An additional multiplier has to be included because the traces were recorded at different attenuations: 15 db for the standard versus 9 db for the target.

86. The emissivity measurements of sand were taken indoors with heated samples. A 6-mm-diam hole in an aluminium block was filled with the sand, and the block heated. Radiation from the sand was compared with radiation from the painted aluminum surface--both assumed to be at the same temperature. Paint was flat black from Rustoleum with a stated emissivity of $\varepsilon_{stand} = 0.87$. The emissivity of the target ε_t was obtained from

$$\varepsilon_t = \varepsilon_{stand} \frac{n_t - n_b}{n_{stand} - n_b} \quad (\text{for } \varepsilon_{stand} = 0.87) \quad (47)$$

where n_t , n_b , and n_{stand} are the spectral radiances of target, background, and black standard, respectively.

87. An example of the traces obtained from the X-Y plotter is

reproduced in Figure C4. It shows, from top to bottom, curves for the black standard, the target, and the background. All curves were traced twice and exhibit excellent reproducibility. Attenuation for all curves was the same; hence, the signal differences required in Equation 47 can be read directly from the graph.

88. For the emissivity measurements of the rock, a black spot was painted onto the rock surface and the rock heated in an oven. After the rock was removed from the oven, three spectral traces were run quickly: first of the black spot, second of the rock surface, and third of the black spot again. The first and third traces were interpolated and compared with the second to obtain ε_t from the above formula. During the emissivity measurements, the radiometer was focused onto the target surface, thus measuring a target area of approximately 1 square mm.

Results of Emissivity Measurements

89. The emissivity of the grey sand from Klondike Flats is shown in Figure 16. There is a gap in the curve at 8 μm and an overlap around 5 μm because of changes in filter wheel segments or detectors. The

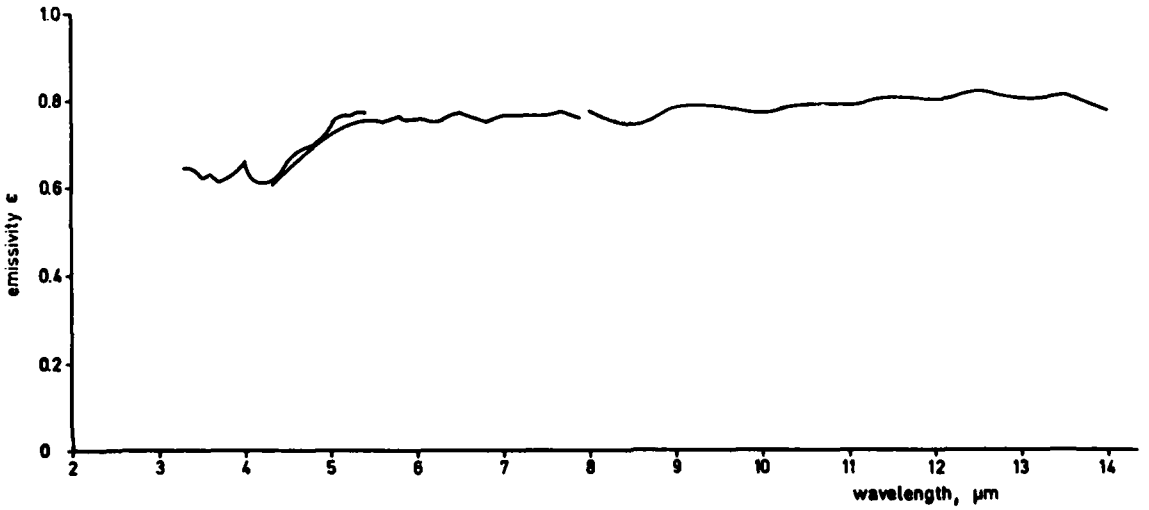

Figure 16. Spectral emissivity for grey sand from Klondike Flats

emissivity turns out to be very flat, with values between 0.75 and 0.80 except for a drop to 0.60 at around 4 μm.

90. Figure 17 shows emissivity for the red sand and the plain

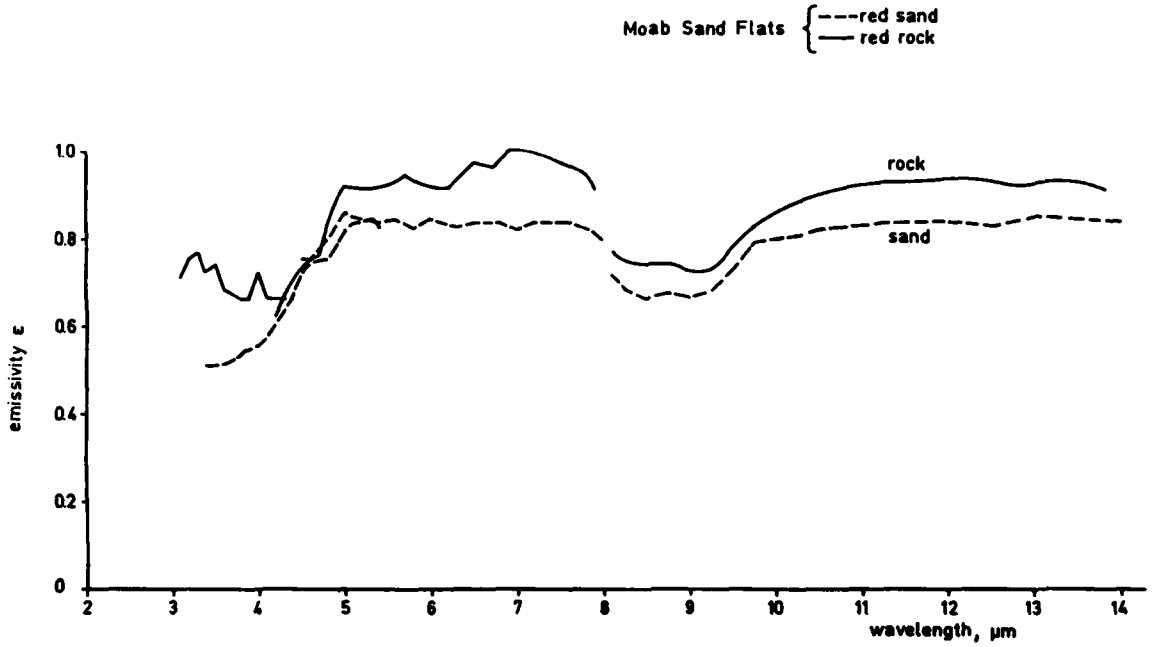

Figure 17. Spectral emissivity for red sand and rock from Sand Flats

rock from Sand Flats. The curve for sand has been obtained from the X-Y plot in Figure C4. Both curves have a dip around 9 μm, which is characteristic for an absorption band of silicates. Both curves parallel each other except at wavelengths below 4.3 μm, where the differences in surface structure apparently become important. Emissivities for the plain rock surface as well as the parts covered with lichen are compared in Figure 18. The lichens caused the absorption band at 9 μm to disappear.

Results of Reflectance Measurements

91. In many cases, reflectance is strongly dependent on the angles of incident and reflected radiation. Extensive measurements were taken of the red sand from Sand Flats in order to find variations

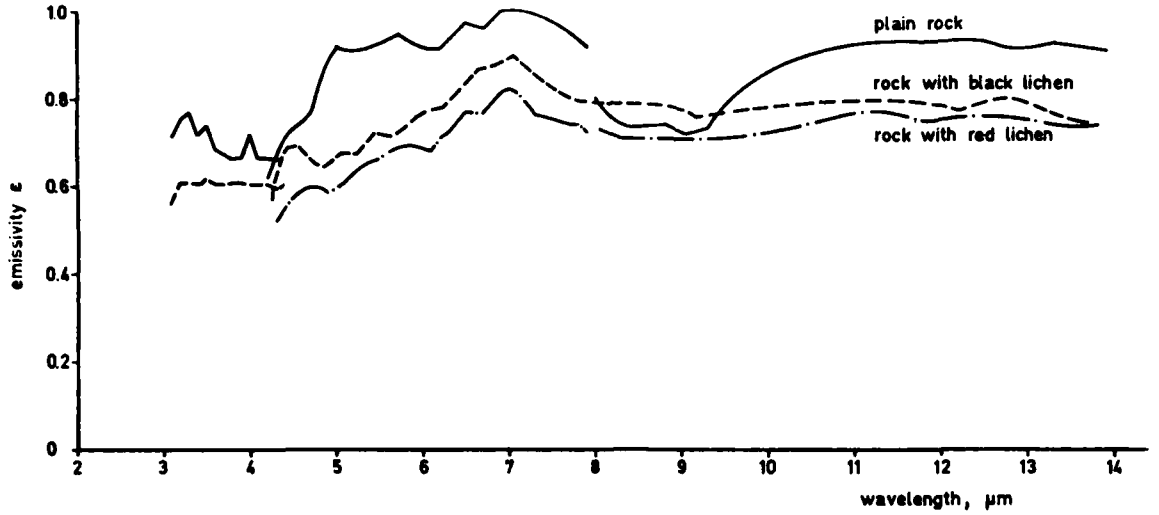

Figure 18. Spectral emissivity for red sandstone from Sand Flats. Rock surface was plain or covered with red or black lichens

in angular reflectance. No significant differences were found for angles larger then 40° above horizontal.

92. Results for spectral reflectances of red sand are given in Figure 19. All values are reflectance factors relative to barium sulfate and were obtained from the X-Y plot in Figure C3. Two cases are shown: forward and backward scattering. In the first the radiometer faces the sun; in the second the sun is behind the radiometer. It is surprising (see Figure 19) that the reflectance for backward scattering is slightly larger than that for forward scattering; however, the difference is not considered significant. Reflectance values for $\lambda = 0.6 - 0.7$ μm are unusually high--around 39 percent--but indicative of the deep red color of the sand. Near infrared reflectance is also quite high.

93. Figure 20 gives spectral reflectance values for the grey sand from Klondike Flats. During the measurement, the incident and reflected beams had an elevation of 60° above horizontal and an azimuth difference of 70°. In comparison with the red sand (see Figure 19), the grey sand has much lower reflectance, especially in the red part of the spectrum and in the near infrared.

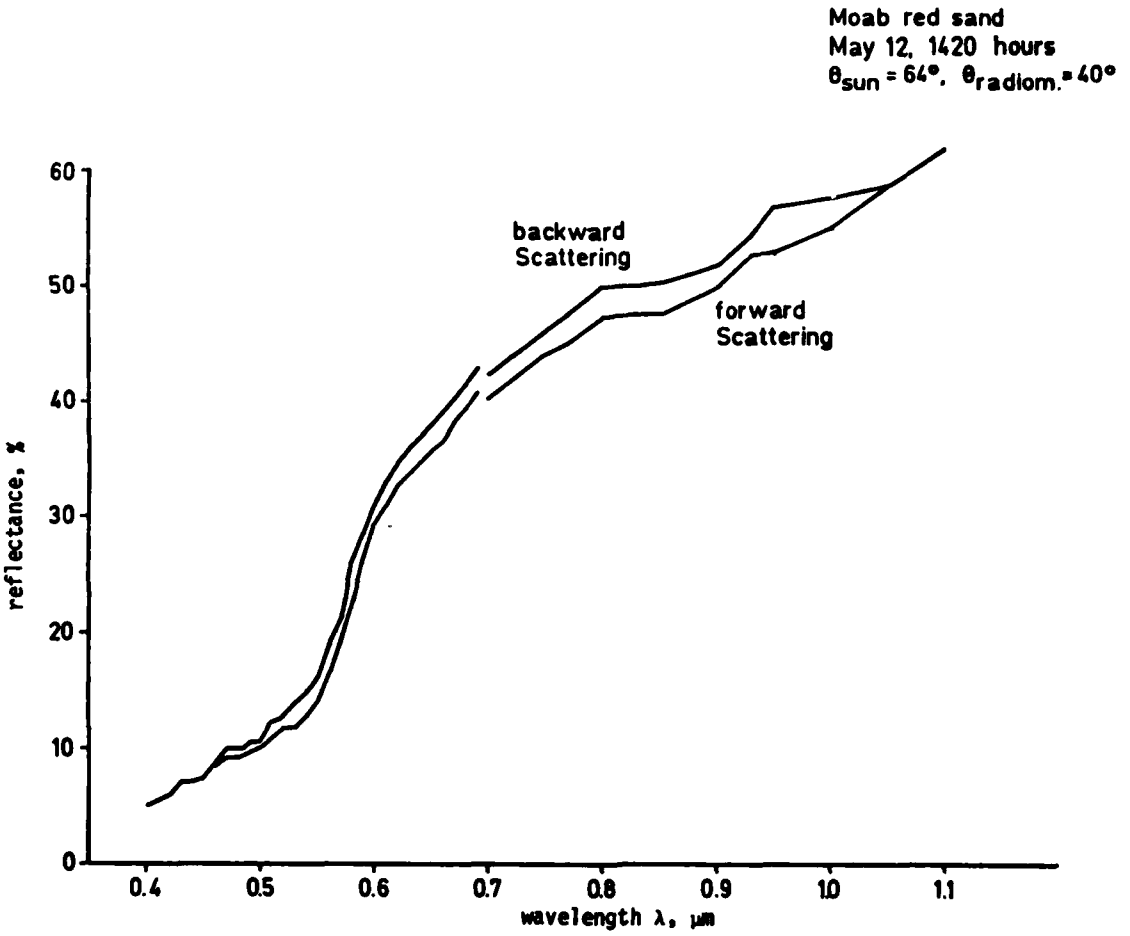

Figure 19. Spectral reflectance for red sand from Sand Flats

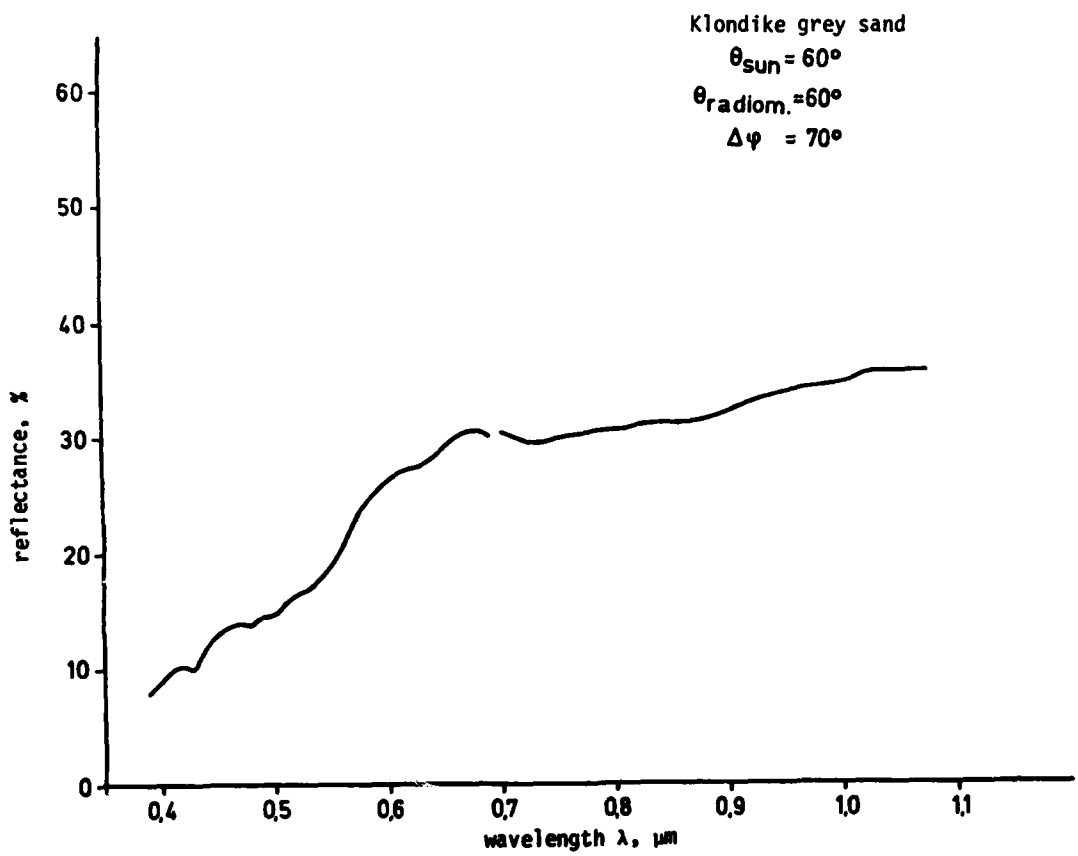

Figure 20. Spectral reflectance for gray sand from Klondike Flats

Evaluation of Desert Measurements

94. The measurements reported here are based on comparisons with a reference surface. The accuracy of the results obtained will depend both on the reference and the instrumentation for measurement.

95. Reproducibility of the measurements was found to be good. Precision of the measurements should be adequate whenever the detector returned a useful signal. This can be evaluated from the signal plots in Figures C3 and C4, Appendix C. Reflectance measurements will be doubtful for wavelengths shorter than 0.40 μm and longer than 0.95 μm. Emissivity measurements with the HgCdTe detector as used in Figure C4 are limited in practice to wavelengths between 4.2 and 14 μm. Additional measurements with the InSb detector extend the shortwave limit down to 3.2 μm.

96. The major contributor of errors in the results is expected to be the reference surfaces. The accuracy of their nominal reflectance or emissivity values is unknown. In addition, the properties of the references might change over time, as was certainly the case for the white standard which was exposed to blowing red sand in the desert environment. However, no unexposed standards were available to determine the amount of deterioration.

97. Spectral characteristics of some desertic materials from Moab, Utah, have been measured. However, thermal models such as the USAEWES Terrain Surface Thermal Model (TSTM) (Balick et al. 1981) do not require spectral data as input, but rather broadband average values such as solar absorptivity and longwave emissivity. The solar absorptivity equals one minus the solar reflectance and can be obtained from the spectral reflectance by weighting it with the incoming solar radiation. A longwave emissivity can similarly be obtained by weighting the spectral emissivity with the blackbody radiation at, for example, 20°C. The results are as follows:

Surface	Solar Absorptivity, %	Longwave Emissivity, %
Grey sand	74.0	78.0
Red sand	58.0	80.0
Red rock	--	89.0

98. The above solar absorptivity would apply to sea level insolation under a clear sky. At higher altitudes, solar radiation contains a larger proportion of short wavelengths which would cause the effective solar absorptivity to increase for the materials investigated.

99. The longwave emissivity derived includes wavelengths between 3 and 14 μm. It would be desirable to include wavelengths between 14 and 20 μm, since they also contribute to the radiation exchange processes modeled in TSTM. However, there are no detectors readily available which would be sensitive in this spectral region.

PART V: CONCLUSIONS

100. A capability to measure spectral surface properties in the visual, near infrared, and thermal infrared has been developed. The instrumentation can be used to collect data on natural and man-made surfaces.

101. Data collected will be required in several current projects at WES.

a. Thermal models need solar absorptivity and thermal emissivity as input parameters.

b. The thermal behavior of potential camouflage materials is being investigated with both contact thermometers and radiation thermometers; surface emissivity is needed to connect the two types of temperature measurement.

c. Materials with low emissivity appear to be promising candidates for future thermal camouflage measures; their properties have to be measured to support the development.

102. Several limitations of the instrument were found in working with the Barnes SpectralMaster:

a. Even though the instrument was built as a compact, fully enclosed unit suggesting its deployment in the field, it is not a field spectroradiometer. The instrument works best in air-conditioned surroundings. In hot, dry desert environments as well as during the hot, humid weather at WES in Vicksburg, Miss., the mechanism rotating the filter wheel performed irregularly or not at all. Returning the instrument to an air-conditioned laboratory cured the malfunctions.

b. Difficulty in handling the instrument also discourages field use. Interchange of the different detectors and filter wheels is not a simple task. Cooling of the detectors is accomplished with high-pressure nitrogen instead of liquid nitrogen and therefore requires a connection to the heavy nitrogen bottle during measurements.

c. The useful wavelength range of the silicon detector is narrower than expected. It should extend up to 1.1 μm in the near infrared, but a damage spot in the filter wheel at 0.97 μm and the steep drop in sensivity beyond this spot limit most measurements to wavelengths below 0.95 μm.

d. The InSb detector was found to be not very useful. It was purchased to extend the sensitivity of the HgCdTe detector to shorter wavelengths. The HgCdTe is sensitive down to about 4.2 μm and the InSb detector extends this only to 3.2 μm. While the infrared filter wheel is well matched to the sensitivity range of the HgCdTe detector, it is poorly matched to the InSb detector explaining the limited extension. Since it is not easy to change detectors, the InSb detector will be used only if there is a particular interest in the wavelength region between 3 and 4 μm.

REFERENCES

Balick, L. K., et al. 1981. "Thermal Modeling of Terrain Surface Elements," Technical Report EL-81-2, U. S. Army Engineer Waterways Experiment Station, CE, Vicksburg, Miss.

Barnes Engineering Company. 1977. "SpectralMaster Infrared Research Radiometer Model 12-550: Instruction Manual, Calibration and Specification Data," Stanford, Md.

_____. 1979. "Handbook of Infrared Radiation Measurement," Stanford, Md.

Buettner, K., Kern, C. D. 1965. "The Determination of Infrared Emissivities of Terrestrial Surfaces," J. Geophysical Res., Vol 70, pp 1329-1337.

Lorenz, D. 1966. "The Effect of Long-Wave Reflectivity of Natural Surfaces on Surface Temperature Measurements Using Radiometers," J. Appl. Meteorology, Vol 5, pp 421-430.

Richmond, J. C. 1980. "Reflectance Errors in Infrared Thermography," Appl. Optics, Vol 19, pp 834-836.

Richter, W. 1980. "Vermessung von IR-Tarnmaterialien," IABG-report B-TU 2009/00, Ottobrunn, Germany.

Wolfe, W. L., Zissis, G. J. 1978. The Infrared Handbook, ERIM, Ann Arbor, Mich.

Table 1

Spectral Data Report for Infrared Filter Segments

Theta*	Lambda θ	HBW	VHBW	Theta'	Lambda'θ	Deviation	Segment
5.	2.5470	0.9296	0.0902	5.	2.4856	2.4711	
15.	2.6757	0.6341	0.2053	15.	2.7242	-1.7803	
30.	3.0606	0.8845	0.0451	30.	3.0822	-0.6931	
45.	3.4248	0.8836	0.0442	45.	3.4401	-0.4436	SEG I
60.	3.8038	0.8749	0.0354	60.	3.7980	0.1515	
75.	4.1692	0.8422	0.0027	75.	4.1560	0.3172	
85.	4.3995	0.8271	0.0123	85.	4.3946	0.1122	
Average HBW =		0.8394					
5.	4.3394	1.0805	0.0540	5.	4.2997	0.9216	
15.	4.7231	1.2138	0.0793	15.	4.4766	-0.4957	
30.	5.3984	1.1930	0.0585	30.	5.4169	-0.3400	
45.	6.0790	1.0638	0.0707	45.	6.0871	-0.1335	SEG II
60.	6.7508	1.1409	0.0064	60.	6.7574	-0.0977	
75.	7.4258	1.1287	0.0058	75.	7.4277	-0.0256	
85.	7.8935	1.1208	0.0136	85.	7.8746	0.2410	
Average HBW =		1.1345					
5.	8.1961	1.3851	0.2722	5.	8.2331	-0.4492	
15.	9.0232	1.2812	0.1683	15.	9.0365	-0.1474	
30.	10.2595	1.2824	0.1695	30.	10.2417	0.1738	
45.	11.4874	1.2061	0.0932	45.	11.4468	0.3548	SEG III
60.	12.6937	0.5331	0.5798	60.	12.6519	0.2299	
75.	13.8816	1.1105	0.0024	75.	13.8571	0.1771	
85.	14.5861	0.9918	0.1211	85.	14.6605	-0.5072	
Average HBW =		1.1129					

* Column explanations:

Theta = angular position on filter in degrees.
Lambda θ = bandpass center wavelength in microns, at positions Theta.
HBW = bandpass width at the halfpower points in percent of Lambda.
VHBW = (average HBW) - HBW.
Theta' = angular position for purposes of best fit straight line.
Lambda'θ = center wavelength values for best fit straight line, Lambda'θ = K · Theta' (K = transfer function).
Deviation = (Lambda θ - Lambda'θ) · 100/Lambda θ.

Table 2

Spectral Data Report for Visible and Near Infrared Filter Segments

Theta*	Lambda θ	HBW	VHBW	Theta'	Lambda'θ	Deviation	Segment
5.	0.6723	2.5433	0.1418	5.	0.6709	0.2189	
15.	0.7197	4.0159	1.6143	15.	0.7163	0.4736	
30.	0.7803	2.4732	0.0717	30.	0.7843	-0.5065	
45.	0.8463	2.3985	0.0030	45.	0.8524	-0.7083	
60.	0.9207	2.4656	0.0641	60.	0.9205	0.0215	
75.	0.9925	2.4587	0.0671	75.	0.9885	0.3979	
90.	1.0592	2.3414	0.0601	90.	1.0566	0.2479	SEG A
105.	1.1260	2.3534	0.0481	105.	1.1246	0.1249	
120.	1.1926	2.2892	0.1123	120.	1.1927	-0.0134	
135.	1.2593	2.2474	0.1542	135.	1.2608	-0.1209	
150.	1.3263	2.2997	0.1018	150.	1.3288	-0.1949	
165.	1.3934	2.2247	0.1768	165.	1.3969	-0.2508	
175.	1.4471	1.0988	1.3028	175.	1.4423	0.3307	
	Average HBW = 2.4015						
Lambda = 0.6482 + (0.00454 · Theta)							
5.	0.3820	4.1105	1.4500	5.	0.3729	2.4186	
15.	0.3956	3.7669	1.1064	15.	0.3927	0.7355	
30.	0.4200	3.2147	0.5542	30.	0.4223	-0.5470	
45.	0.4491	2.7830	0.1225	45.	0.4519	-0.5991	
60.	0.4782	2.5724	0.0881	60.	0.4815	-0.6864	
75.	0.5066	2.3293	0.3312	75.	0.5111	-0.8712	
90.	0.5359	2.4820	0.1785	90.	0.5407	-0.8878	SEG B
105.	0.5686	2.1986	0.4619	105.	0.5702	-0.2976	
120.	0.5996	2.2850	0.3755	120.	0.5998	-0.0492	
135.	0.6300	2.2540	0.4065	135.	0.6294	0.0886	
150.	0.6600	2.2727	0.3878	150.	0.6590	0.1457	
165.	0.6900	2.1159	0.5446	165.	0.6885	0.1978	
175.	0.7132	2.2015	0.4590	175.	0.7084	0.6749	
	Average HBW = 2.6605						
Lambda = 0.3631 + (0.00197 · Theta)							

* Column explanations:

Theta = angular position on filter in degrees.
Lambda θ = bandpass center wavelength in microns, at position Theta.
HBW = bandpass width at the halfpower points in percent of Lambda.
VHBW = (average HBW) - HBW.
Theta' = angular position for purposes of best fit straight line.
Lambda'θ = center wavelength values for best fit straight line,
Lambda'θ = K · Theta' (K = transfer function).
Deviation = (Lambda θ - Lambda'θ) · 100/Lambda θ .

Table 3

Wavelength Calibration of Filter Wheels

Infrared

Dial reading d is a function of output voltage V_x

$$d = 10.16 + 13.17\ V_x \quad (1)$$

SEG I

$$\lambda = 0.0239 \cdot \theta + 2.366 \quad (6)$$
$$= 0.0273 \cdot d + 2.165 \quad \theta = \frac{d - 7.38}{0.875} \quad (7)$$
$$= 0.359 \cdot V_x + 2.442 \quad (5)$$

SEG II

$$\lambda = 0.0447 \cdot \theta + 4.076 \quad (3)$$
$$= 0.0496 \cdot d - 2.181 \quad \theta = \frac{d - 126.1}{0.90} \quad (4)$$
$$= 0.654 \cdot V_x - 1.677 \quad (2)$$

SEG III

$$\lambda = 0.0801 \cdot \theta + 7.848$$
$$= 0.0910 \cdot d - 14.489 \quad \theta = \frac{d - 245.5}{0.88} \quad (8)$$
$$= 1.198 \cdot V_x - 13.565$$

Visual and Near Infrared

Dial reading d is a function of output voltage V_x

$$d = 11.37 + 13.27\ V_x \quad (9)$$

SEG A (visual)

$$\lambda = 0.024\ V_x + 0.395 \quad (14)$$
$$= 0.00197\ \theta + 0.363 \quad (16) \quad \theta = \frac{d + 6.13}{1.0875} \quad (17)$$
$$= 0.00181\ d + 0.374 \quad (15)$$

SEG B (near infrared)

$$\lambda = 0.0563\ V_x - 0.079 \quad (10)$$
$$= 0.00454\ \theta + 0.648 \quad (11) \quad \theta = \frac{d - 182.9}{1.071} \quad (13)$$
$$= 0.00424\ d - 0.127 \quad (12)$$

Table 4

Summary of Relative Response R for Infrared Filter Wheel and HgCdTe Detector

Filter Segment	Wave-Length λ μm	Filter Transmission τ A* % μm	Filter Transmission τ B** % μm	Detector Response D	Relative Response R R = B · D % μm	Relative Response R R = B · D % of Max
SEG I	2.5470	1.18	1.20	0.385	0.463	7.35
	2.6751	0.88	1.24	0.340	0.420	6.67
	3.0606	1.73	1.77	0.257	0.455	7.22
	3.4248	2.12	2.26	0.273	0.618	9.81
	3.8038	2.23	2.25	0.315	0.709	11.25
	4.1692	2.11	2.16	0.370	0.801	12.71
	4.3995	1.60	1.66	0.410	0.680	10.80
SEG II	4.3394	2.40	2.45	0.400	0.979	15.50
	4.7231	2.49	2.48	0.460	1.141	18.10
	5.3984	2.99	2.99	0.555	1.660	26.30
	6.0790	3.30	3.89	0.640	2.490	39.50
	6.7506	4.27	4.55	0.730	3.320	52.70
	7.4258	4.69	5.10	0.808	4.120	65.40
	7.8935	4.78	4.93	0.850	4.190	66.50
SEG III	8.1961	4.27	4.61	0.885	4.080	64.80
	9.0232	5.46	5.83	0.937	5.460	86.80
	10.2595	5.65	6.14	0.993	6.100	96.70
	11.4874	6.24	6.52	0.965	6.300	100.00
	12.6937	2.98	6.75	0.690	4.660	74.00
	13.8816	6.09	6.72	0.300	2.020	32.10
	14.5861	4.73	4.83	0.008	0.040	0.63

* Determined from triangular approximation.
** Determined planimetrically.

Table 5

Relative Response R for Visual and Near Infrared Filter Wheel and Si Detector

Filter Segment	Wavelength λ μm	Filter Transmission τ % μm	Detector Response D %	Relative Response R = τD, % μm
SEG A	0.3820	0.234	38.0	0.089
	0.3956	0.274	39.5	0.108
	0.4200	0.314	44.0	0.138
	0.4491	0.299	51.0	0.153
	0.4782	0.292	67.5	0.197
	0.5066	0.292	81.0	0.237
	0.5359	0.299	87.0	0.260
	0.5680	0.285	91.5	0.261
	0.5996	0.307	97.0	0.297
	0.6300	0.307	98.5	0.302
	0.6600	0.331	100.0	0.331
	0.6900	0.350	100.0	0.350
	0.7132	0.394	98.0	0.386
SEG B	0.6723	0.510	100.0	0.510
	0.7146	0.733	97.0	0.711
	0.7803	0.733	84.0	0.616
	0.8463	0.698	78.0	0.544
	0.9207	0.719	92.2	0.663
	0.9925	0.698	82.0	0.572
	1.0592	0.768	30.0	0.230
	1.1260	0.789	10.0	0.079
	1.1926	0.768	2.5	0.019

Table 6

Measured Values of Transfer Function t and Derived System Response Factors

Segment	Wavelength μm	Transfer Function, $\frac{Vm^2\Omega\mu m}{W}$					System Response Factor, $\frac{Vm^2\Omega}{W}$			
		Source Temperature, °C					Source Temperature, °C			
		25	100	180	200	Average	25	100	180	200
SEG I	3.8028	--	0.041	0.045	0.046	0.044	--	5.7	6.4	6.5
SEG II $t_{ref} = 60°$	4.3394	0.070	--	--	--	0.070	7.2	--	--	--
	4.7231	0.098	0.102	0.105	0.106	0.103	8.6	8.9	9.2	9.2
	5.3984	0.143	0.119	0.129	0.129	0.130	8.6	7.2	7.8	7.8
	6.0790	0.199	--	--	--	0.199	8.0	--	--	--
	6.7506	0.252	--	--	--	0.252	7.6	--	--	--
	7.4258	0.313	--	--	--	0.313	7.6	--	--	--
	7.8935	0.310	0.287	0.299	0.298	0.298	7.4	6.8	7.1	7.1
SEG III $t_{ref} = 65°$	8.1961	0.306	0.302	0.307	0.300	0.304	7.5	7.4	7.5	7.4
	9.0732	0.383	0.372	0.375	0.370	0.375	7.0	6.8	6.9	6.8
	10.2595	0.414	0.439	0.449	0.450	0.438	6.8	7.2	7.4	7.4
	11.4874	0.384	0.375	0.408	0.404	0.393	6.1	6.0	6.5	6.4
	12.6937	0.238	0.216	0.246	0.247	0.237	5.1	4.6	5.3	5.3
	13.8816	0.040	0.060	--	0.084	0.061	2.0	3.0	--	4.1
	14.5861*	--	--	--	--	--	--	--	--	--

* Weak signal: no data.

APPENDIX A: OPERATING SEQUENCE FOR BARNES SPECTRALMASTER 12-550

1. The following sequence emphasizes those points that are not well covered in the Barnes Instruction Manual (1977). Frequent references to this manual are abbreviated as B.

a. Mount sensing head on tripod.

b. Remove sensing head covers, see B, p 18.

c. Check whether desired detector and filter wheel are installed and connected.
If YES go to 9.

d. Remove filter wheel, see B, p 70.

e. Remove detector module, see B, p 20.

f. Change relay lens to Irtran IV for HgCdTe and InSb detector, or to quartz for Si detector.

g. Install desired detector, see B, p 20, and connect it to J102.

h. Install corresponding filter wheel (removing the tape cover from all three openings), see B, p 20, and connect it to J103 and to the banana plug.

i. Replace the sensing head covers, see B, p 23.

j. Open the front panel of the electronic control unit and set the three accessible switches as follows:

For Detectors	Center Switch S1	Rotary at Far Left	Bat Handle at Far Left
Si	Si	Si	Invert
InSb	InSb	InSb	Invert
HgCdTe	HgCdTe	Spare	Invert

k. Connect sensing head to electronic control unit and plug in electronic control unit.

l. Connect outputs of the electronic control unit (J2, J3) to an X-Y plotter and/or to two voltmeters. For convenience use the Hewlett-Packard plotter with a vertical sensitivity of 1 V/inch and a horizontal sensitivity of 2.6 V/inch. Chart paper has been developed for this setting--see Appendix C, Figures C1 and C2. The paper shows two lines for setting the zero of the X-axis: one for manual and one for automatic recordings. However, since the speed of the filter wheel motor varies, it

is advisable in automatic recordings to adjust the setting by checking the location of a convenient absorption band. If the Si detector is used, go to 17.

m. Obtain a high-pressure nitrogen bottle and secure it so it cannot topple over.

n. Remove bottle cover, install a pressure regulator, and connect it with a high-pressure hose to the inlet at the detector. When disconnected, the inlet at the detector should always be protected with the yellow cap. This prevents moisture contamination of the molecular sieve.

o. Flush the detector at a pressure of 50 psi for 10-15 min to remove residual moisture.

p. Raise pressure to 1500 psi.

q. Power the radiometer by turning the output bandwidth switch to 1 Hz, and allow for a warm-up of several minutes.

r. To aim the radiometer at the target, move the slide on the sensing head to "closed" and look through the eyepiece. Focus the radiometer by turning the knurled knob. Depth of focus is very narrow, and it may require some patience to find the target. If focused, the radiometer measures only the area within the small circle of the eyepiece.

s. Most measurements will be taken with the instrument settings as follows:

(1) ETO: OFF

(2) Output bandwidth: 1 Hz (response at 0.1 Hz is too slow)

(3) Slide on sensing head: open

(4) Attenuator: 3-12 db (Si and HgCdTe detector)

12-36 db (InSb detector)

The attenuation factors corresponding to these attenuator control settings are given in B, p 46.

Moving the toggle switch on the electronic control unit to the left or right activates the filter wheel motor.

APPENDIX B: TRANSMISSION OF FILTER SEGMENTS

1. The following figures provide the data on filter transmission for segments SEG A, SEG B, SEG I, SEG II, SEG III.

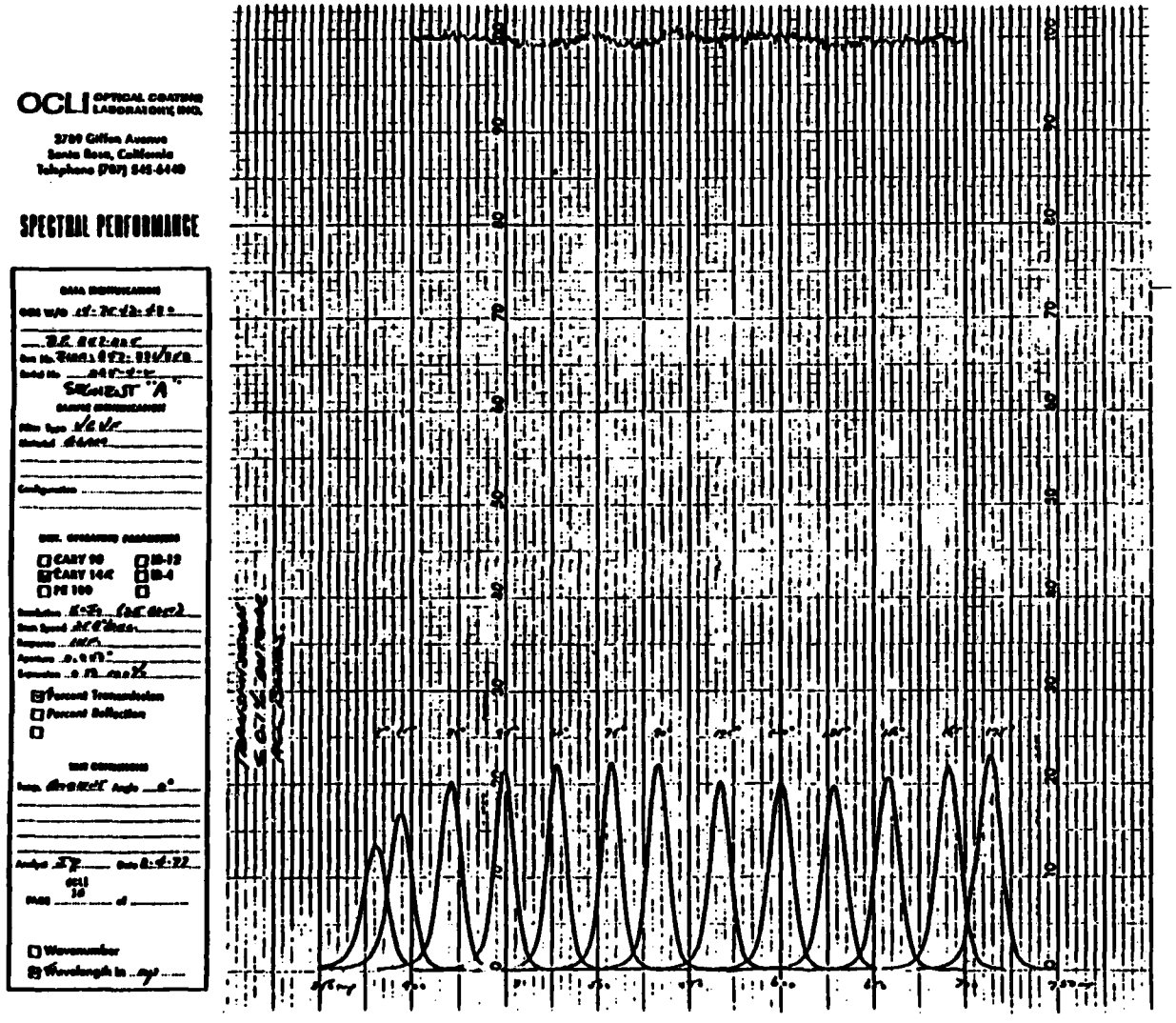

Figure B1. Filter transmission data for SEG A

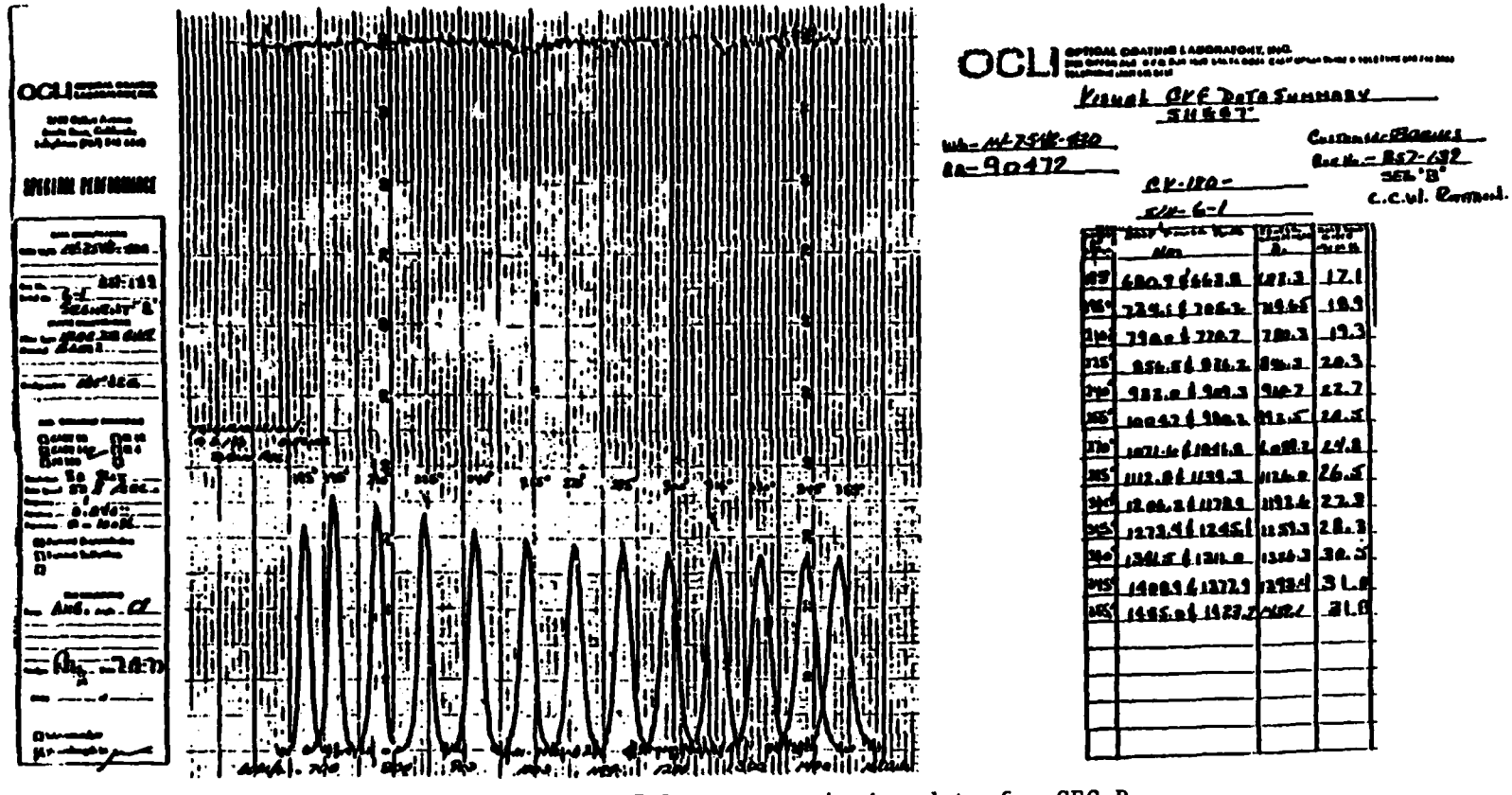

Figure B2. Filter transmission data for SEG B

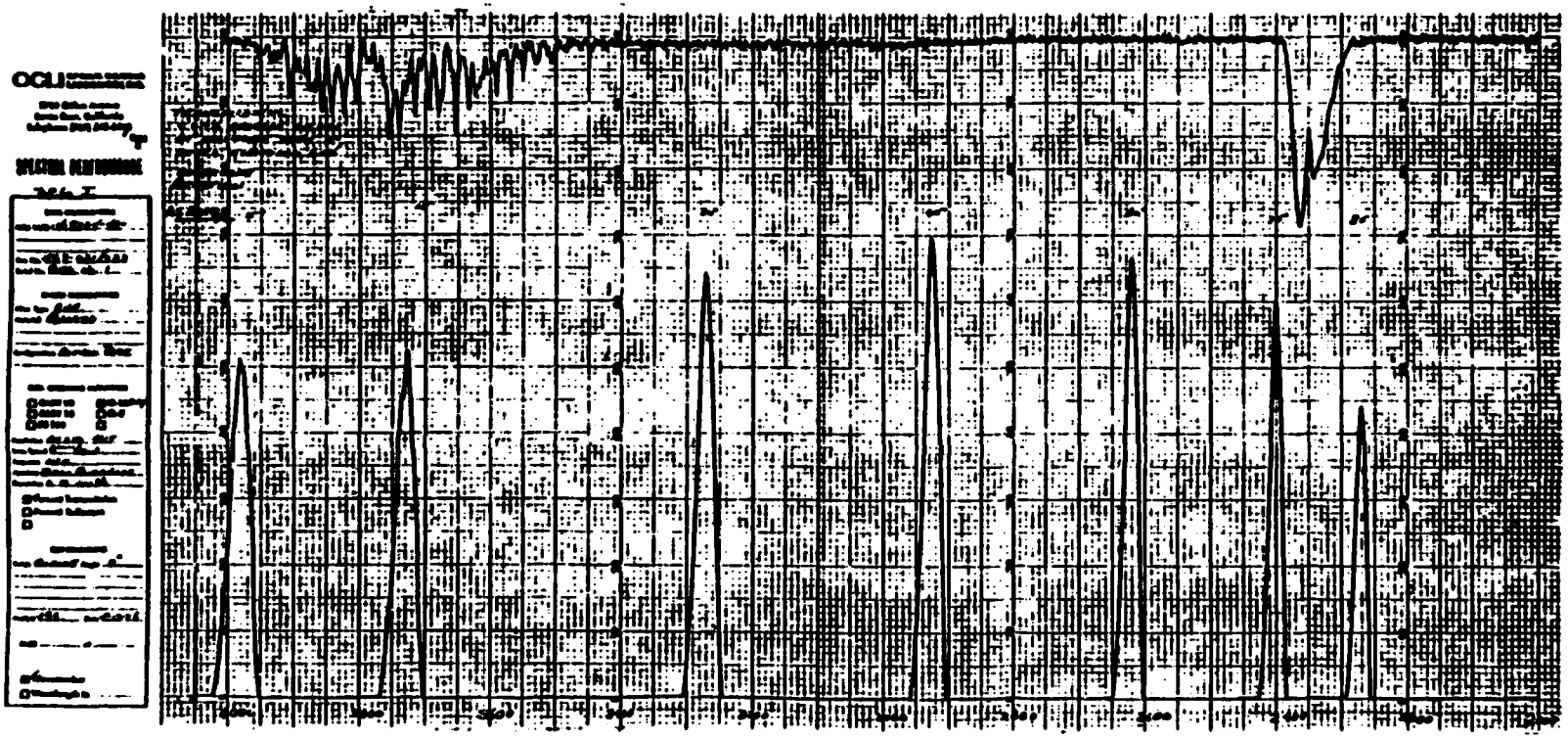

Figure B3. Filter transmission data for SEG I

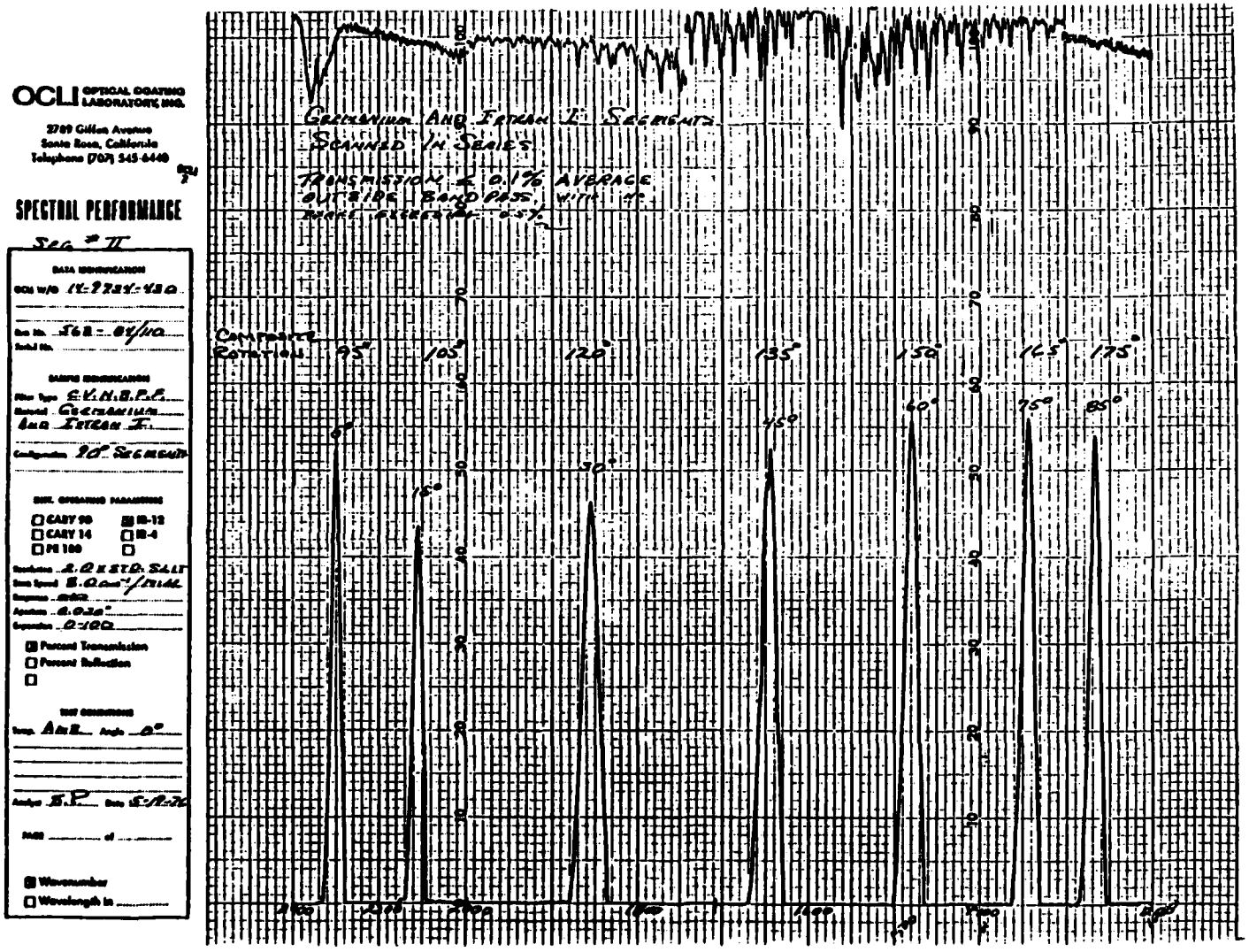

Figure B4. Filter transmission data for SEG II

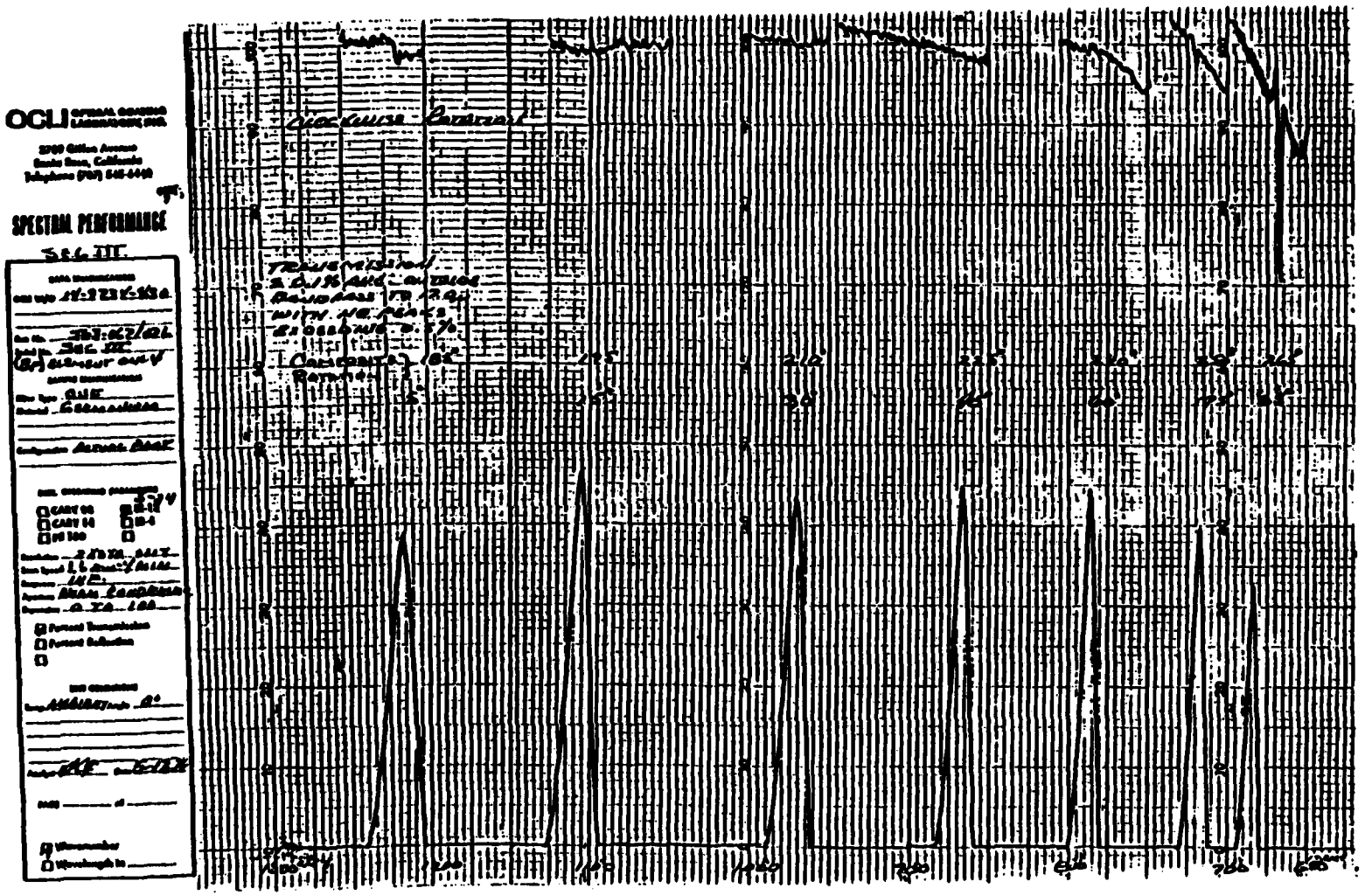

Figure B5. Filter transmission data for SEG III

APPENDIX C: X-Y PLOTTER: EXAMPLES FOR GRAPH PAPER AND SIGNAL PLOTS

1. The following pages show examples of the graph paper to be used with a Hewlwtt-Packard X-Y plotter. Figures C1 and C2 are plain data sheets for the visual and near infrared (SEG A, SEG B) and for the thermal infrared (SEG I, II, III), respectively. Figures C3 and C4 are copies of actual measured curves.

2. Measurements of reflectance for red sand are reproduced in Figure C3. One curve has been traced for the white standard and four curves for sand relating to four different angles of reflectance. The curves have been traced at attenuation settings of 15 and 9 db to make good use of the vertical scale. All traces go off scale at the damage spot for $\lambda = 0.97\ \mu m$, which is of no concern since the graph does not contain any useful information at this point.

3. An emissivity measurement for red sand is shown in Figure C4. There are three curves: for room temperature background, for the heated red sand, and for a painted reference heated to the same temperature. This temperature was approximately 110° C. The signal from the background is negative because its temperature is less than that of the internal reference cavity of the radiometer. All three curves have been traced twice, displaying excellent reproducibility.

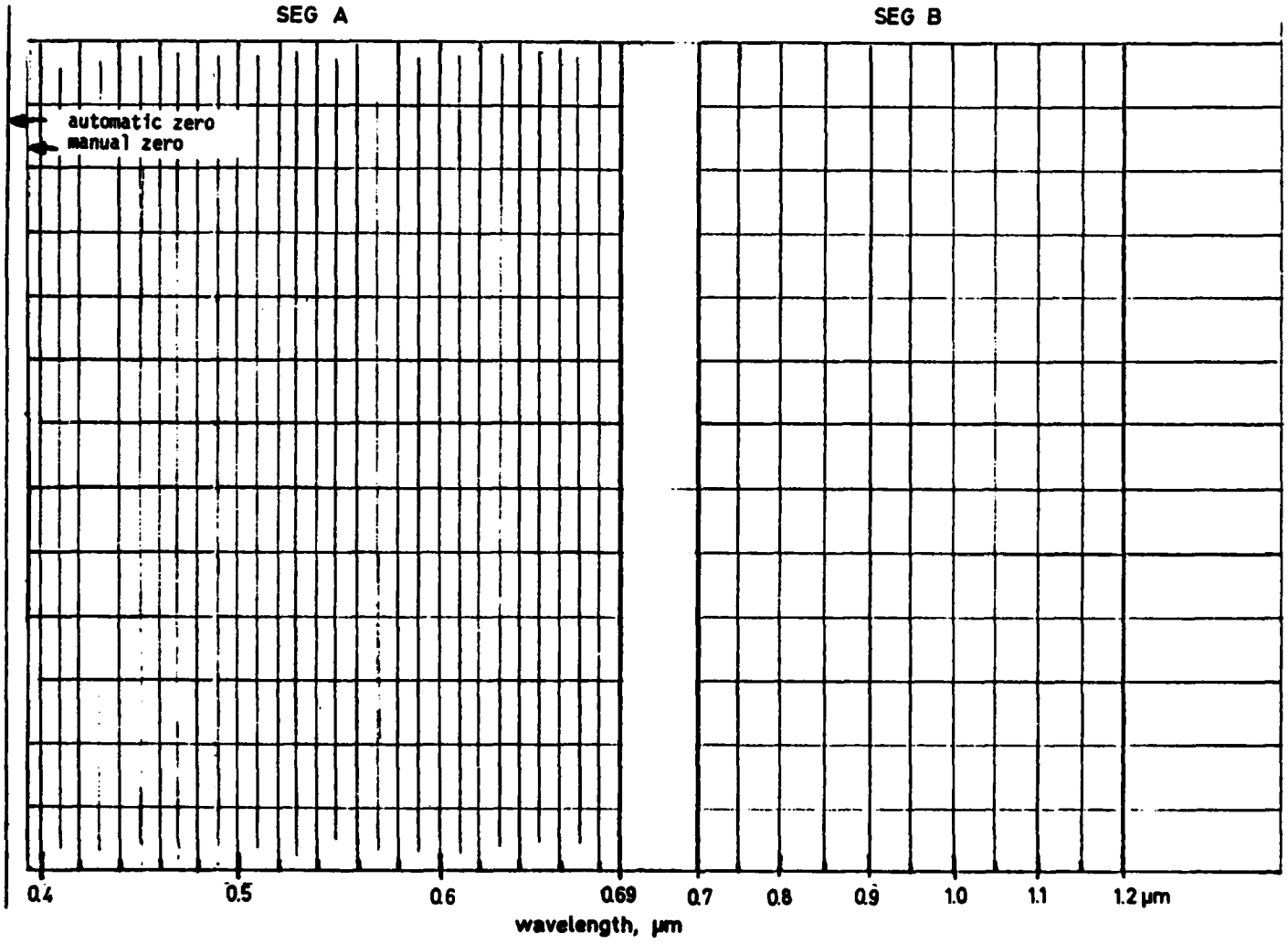

Figure C1. Plain data sheets for the visual and near infrared to be used with a Hewlett-Packard X-Y plotter

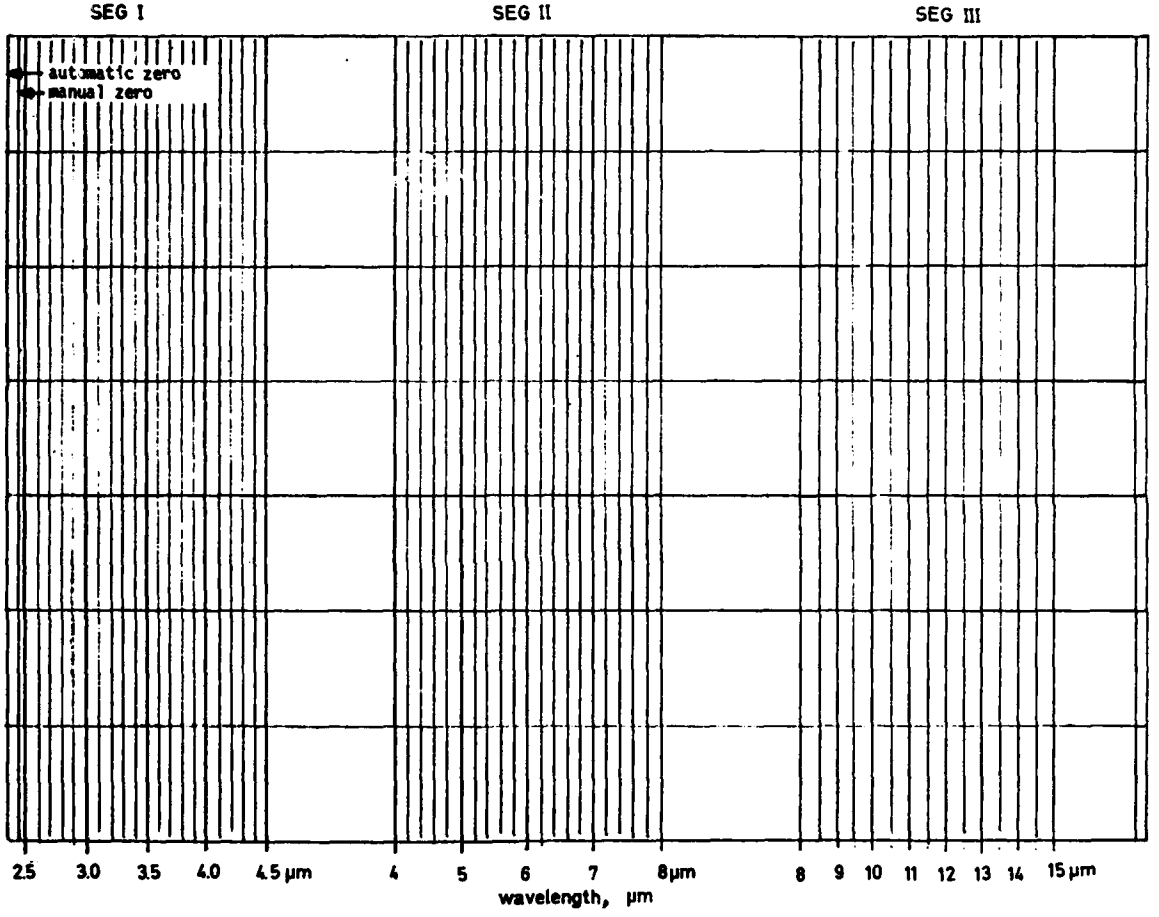

Figure C2. Plain data sheets for the thermal infrared for use with a Hewlett-Packard X-Y plotter

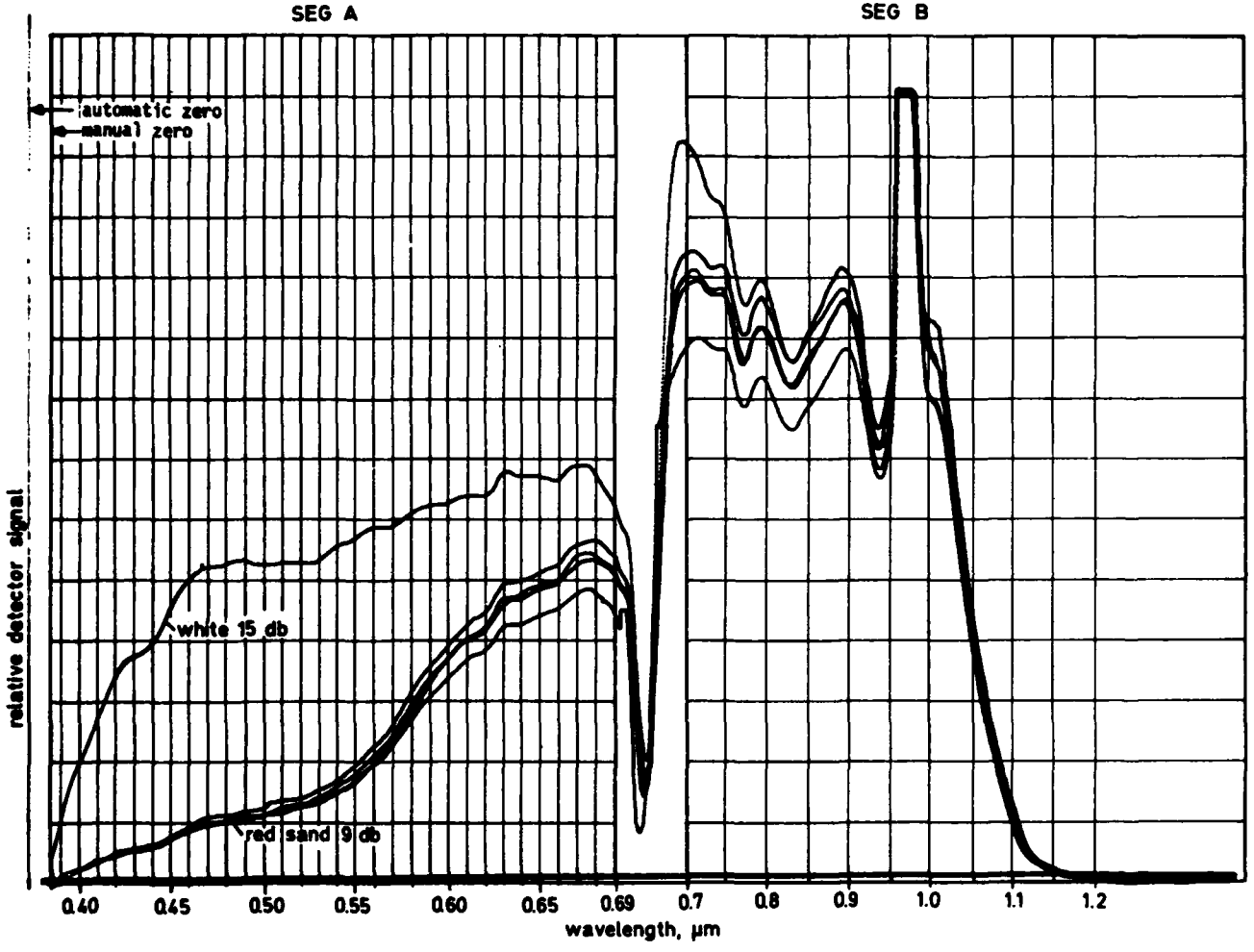

Figure C3. Reflectance curves measured for red sand and the white standard, Moab, Utah

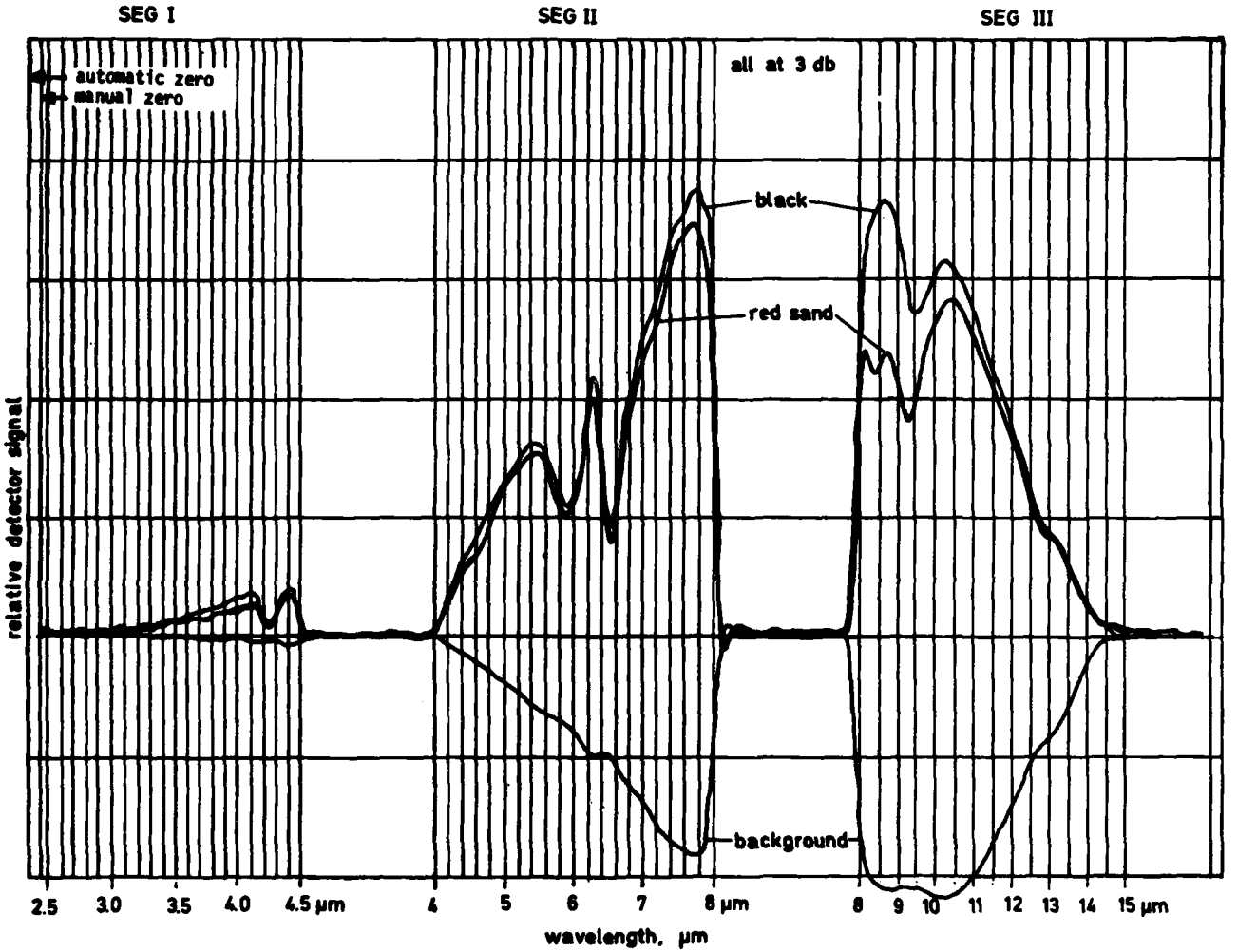

Figure C4. Emissivity curves measured for the black standard, red sand, and background, Moab, Utah

In accordance with letter from DAEN-RDC, DAEN-ASI dated 22 July 1977, Subject: Facsimile Catalog Cards for Laboratory Technical Publications, a facsimile catalog card in Library of Congress MARC format is reproduced below.

Hübner, Gunter
Spectral measurements of reflectance, radiance, and emissivity / by Gunter Hübner (Environmental Laboratory, U.S. Army Engineer Waterways Experiment Station). -- Vicksburg, Miss. : The Station ; Springfield, Va. ; available from NTIS, 1982.
72 p. in various pagings ; ill. ; 27 cm. -- (Technical report ; EL-82-8)
Cover title.
"October 1982."
Final report.
"Prepared for Office, Chief of Engineers, U.S. Army under Project No. 4A762730AT42, Task E3, Work Unit 002."
Bibliography: p. 53.

1. Camouflage (Military science). 2. Military art and science. 3. Spectrum analysis. I. United States. Army. Corps of Engineers. Office of the

Hubner, Gunter
Spectral measurements of reflectance, radiance : ... 1982.
(Card 2)

Chief of Engineers. II. U.S. Army Engineer Waterways Experiment Station. Environmental Laboratory. III. Title IV. Series: Technical report (U.S. Army Engineer Waterways Experiment Station) ; EL-82-8.
TA7.W34 no.EL-82-8

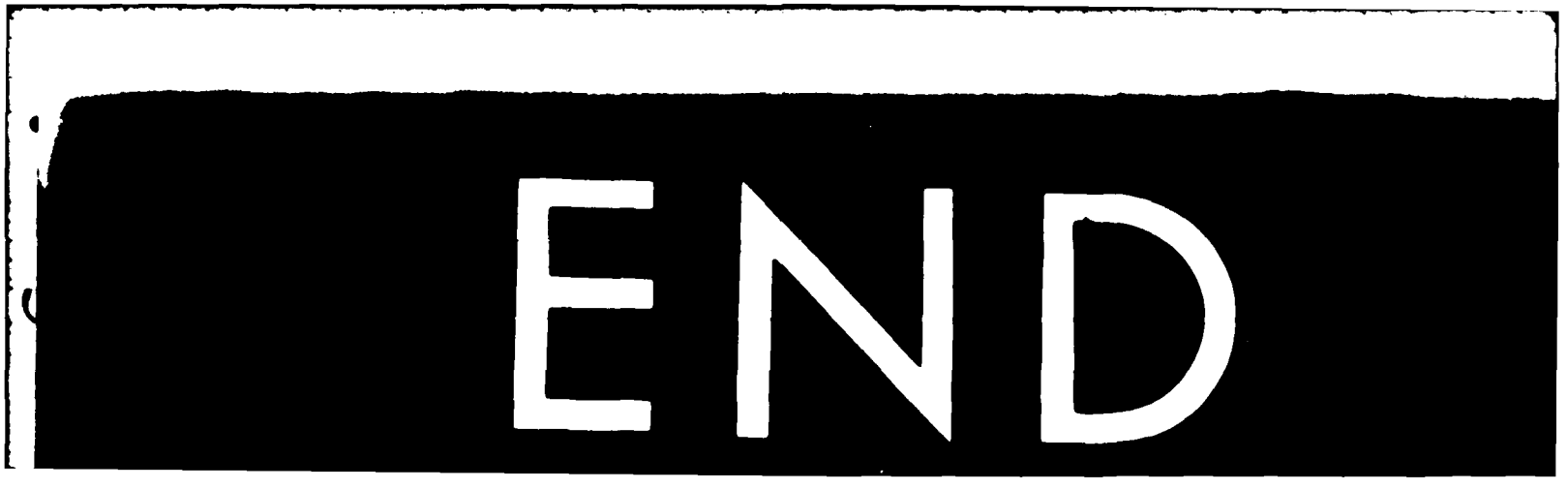
END